


Fall 2004

# Biomimetic synthesis within polyelectrolyte microcapsules: Characterization of enzyme catalyzed polyphenols and polypeptides

Rohit C. Ghan  
*Louisiana Tech University*

Follow this and additional works at: <https://digitalcommons.latech.edu/dissertations>

 Part of the [Biomedical Engineering and Bioengineering Commons](#), and the [Chemical Engineering Commons](#)

---

## Recommended Citation

Ghan, Rohit C., "" (2004). *Dissertation*. 604.  
<https://digitalcommons.latech.edu/dissertations/604>

This Dissertation is brought to you for free and open access by the Graduate School at Louisiana Tech Digital Commons. It has been accepted for inclusion in Doctoral Dissertations by an authorized administrator of Louisiana Tech Digital Commons. For more information, please contact [digitalcommons@latech.edu](mailto:digitalcommons@latech.edu).

# NOTE TO USERS

This reproduction is the best copy available.

**UMI**<sup>®</sup>



**BIOMIMETIC SYNTHESIS WITHIN POLYELECTROLYTE  
MICROCAPSULES: CHARACTERIZATION OF ENZYME  
CATALYZED POLYPHENOLS AND POLYPEPTIDES**

by

Rohit C. Ghan, M.S.

A Dissertation Presented in Partial Fulfillment  
of the Requirements for the Degree  
Doctor of Philosophy

COLLEGE OF ENGINEERING AND SCIENCE  
LOUISIANA TECH UNIVERSITY

November 2004

UMI Number: 3148957

### INFORMATION TO USERS

The quality of this reproduction is dependent upon the quality of the copy submitted. Broken or indistinct print, colored or poor quality illustrations and photographs, print bleed-through, substandard margins, and improper alignment can adversely affect reproduction.

In the unlikely event that the author did not send a complete manuscript and there are missing pages, these will be noted. Also, if unauthorized copyright material had to be removed, a note will indicate the deletion.

**UMI**<sup>®</sup>

---

UMI Microform 3148957

Copyright 2005 by ProQuest Information and Learning Company.

All rights reserved. This microform edition is protected against unauthorized copying under Title 17, United States Code.

ProQuest Information and Learning Company  
300 North Zeeb Road  
P.O. Box 1346  
Ann Arbor, MI 48106-1346

LOUISIANA TECH UNIVERSITY

THE GRADUATE SCHOOL

11/04/2004  
Date

We hereby recommend that the Dissertation prepared under our supervision by Rohit Ghan entitled "*Biomimetic Synthesis Within Polyelectrolyte Microcapsules: Characterization Of Enzyme Catalyzed Polyphenols And Polypeptides*" An Approach towards potential applications of drug delivery and sensors" be accepted in partial fulfillment of the requirements for the Degree of Doctor of Philosophy

Yuqi Luou  
Supervisor of Dissertation Research  
Bill Johnson  
Head of Department  
Chemical Engineering  
Department

Recommendation concurred in:

Yuqi Luou  
Robert A. Libb  
Michael J. McShane  
Bill Johnson  
Yi Sey

Advisory Committee

Approved:  
Bala Ramachandran  
Director of Graduate Studies  
Steve Kopp  
Dean of the College

Approved:  
Terry McConally  
Dean of the Graduate School

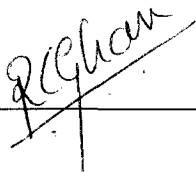
## ABSTRACT

An enzyme-catalyzed synthesis of novel polymers within layer-by-layer (LbL) constructed polyelectrolyte microcapsules has been developed. This approach is based on the selective permeability of polyelectrolyte-capsule walls to monomer molecules. Conversely biocatalysts and forming polymeric chains cannot exit the micro-capsule interior because of their characteristic high molecular weight. Horseradish Peroxidase (HRP) was encapsulated into four bilayer PSS (poly-styrenesulfonate)/ PAH (poly-allylamine hydrochloride) capsules with an average diameter of 5  $\mu\text{m}$  using pH-driven pore opening. The polymerization of 4-(2-Aminoethyl) phenol hydrochloride (tyramine) catalyzed by HRP produces easily detectable fluorescent polymeric products after the addition of hydrogen peroxide to the system. It is known that proteolytic enzymes that effect hydrolysis can be used for peptide synthesis by manipulating physicochemical conditions such as pH, enzyme concentration, oxygen tension, and temperature. Papain (an endolytic cysteine protease, isolated from papaya latex) was encapsulated into four bilayer Tannic acid/ Chitosan capsules with an average diameter of 6  $\mu\text{m}$ . Papain catalyzed polymerization of phenylalanine to its corresponding polymeric form was achieved by heating a mixture of capsules with encapsulated papain within and monomer at 40°C for several hours. The filling of the capsules with polymer was confirmed by AFM (Atomic Force Microscopy), QCM (Quartz Crystal Microbalance), FS (Fluorescence Spectrometry), and CLSM (Confocal Laser Scanning Microscopy). This approach offers a novel biosynthetic pathway for polypeptide synthesis within micron-sized “reactors”, which can have many applications within the field of biotechnology.

## APPROVAL FOR SCHOLARLY DISSEMINATION

The author grants to the Prescott Memorial Library of Louisiana Tech University the right to reproduce, by appropriate methods, upon request, any or all portions of this Dissertation. It is understood that "proper request" consists of the agreement, on the part of the requesting party, that said reproduction is for his personal use and that subsequent reproduction will not occur without written approval of the author of this Dissertation. Further, any portions of the Dissertation used in books, papers, and other works must be appropriately referenced to this Dissertation.

Finally, the author of this Dissertation reserves the right to publish freely, in the literature, at any time, any or all portions of this Dissertation.

  
\_\_\_\_\_  
11/16/04  
\_\_\_\_\_

Author

Date



## TABLE OF CONTENTS

<b>LIST OF TABLES</b> .....	vii
<b>LIST OF FIGURES</b> .....	viii
<b>1. INTRODUCTION</b> .....	1
1.1 Multilayered Polyelectrolyte Microcapsules (PEM)s.....	1
1.2 Enzyme Multilayers on PEMs and Enzyme Encapsulation.....	4
1.3 Enzymatic Catalysis.....	6
1.4 Chemical Reactions Within PEMs.....	8
1.5 Enzyme Catalyzed Polymerization Within PEMs .....	9
1.6 Chapter Outlines .....	10
<b>2. ENZYME CATALYZED SYNTHESIS</b> .....	11
2.1 Historical Perspective on Enzymatic Catalysis.....	11
2.2 Enzyme Catalyzed Polymerization .....	13
2.3 Peroxidase Catalyzed Polymerization .....	14
2.4 Protease Catalyzed Polymerization.....	17
<b>3. MATERIALS AND METHODS</b> .....	20
3.1 Materials .....	20
3.2 MnCO <sub>3</sub> Template Particle Formation .....	23
3.3 Preparation of (PSS/PAH) <sub>4</sub> Microcapsules.....	24
3.4 Encapsulation of HRP in Microcapsules .....	25
3.5 Polymerization Catalyzed by HRP .....	25
3.6 Preparation of [Tannic Acid (TA)/Chitosan (CHW)] <sub>4-5</sub> Hollow Capsules .....	25
3.7 LbL Self Assembly of Papain on QCM Resonator and MnCO <sub>3</sub> Cores.....	26
3.8 Polymerization Catalyzed by Papain on MnCO <sub>3</sub> Cores .....	27
3.9 Encapsulation of Papain in (TA/CHW) <sub>5</sub> in Microcapsules .....	28
3.10 Characterization of Capsules .....	28
<b>4. INSTRUMENTATION</b> .....	30
4.1 QCM Characterization.....	30
4.2 “Zeta-Plus” Potential Measurement.....	34

4.3 Confocal Laser Scanning Microscopy (CLSM) .....	35
4.4 Fluorescence Spectrophotometer .....	37
4.5 Atomic Force Microscope (AFM) .....	38
<b>5. RESULTS AND DISCUSSION .....</b>	<b>39</b>
5.1 Fabrication of (PEM)s and Encapsulation of HRP Within Capsules .....	39
5.2 Polymerization Catalyzed by HRP Within Micro-Capsules.....	40
5.3 Polymerization Catalyzed by HRP Within Micro-Capsules.....	48
5.4 Papain Assembly on MnCO <sub>3</sub> Cores.....	50
5.5 Polymerization of Phenylalanine Catalyzed by Papain Assembled on MnCO <sub>3</sub> Cores .....	52
5.6 Encapsulation of Papain within (TA/CHW) <sub>5</sub> Microcapsules.....	54
<b>6. CONCLUSIONS AND RECOMMENDATIONS.....</b>	<b>57</b>
6.1 Conclusion .....	57
6.2 Recommendations for Future Work.....	58
<b>REFERENCES.....</b>	<b>60</b>
<b>APPENDIX A .....</b>	<b>72</b>
<b>APPENDIX B .....</b>	<b>82</b>
<b>APPENDIX C .....</b>	<b>84</b>

## LIST OF TABLES

Table 1.1 Enzymes commonly used for organic syntheses .....	7
---	---

## LIST OF FIGURES

Figure 1.1: Schematic representation of the capsule formation via LbL assembly, encapsulation of HRP and Papain within the capsules and polymer formation <i>in Situ</i> .....	10
Figure 2.1: Oxidative polymerization of phenol catalyzed by HRP in aqueous dioxane mixture yielding phenylene and oxy-phenylene units .....	15
Figure 3.1: Structural formula for PSS .....	21
Figure 3.2: Structural formula for PAH.....	21
Figure 3.3: Structural formula for Phenylalanine .....	22
Figure 3.4: Structural formula for Glutamic acid .....	22
Figure 3.5: Structural formula for Tannic acid .....	23
Figure 3.6: Structural formula for Chitosan.....	23
Figure 5.1: $\zeta$ potential of polyelectrolytes coated MF particles vs. number of adsorbed layers. The dashed and solid lines represent data of two independent experiments on assembling (PSS/PAH) <sub>4</sub> layers on MF cores .....	40
Figure 5.2: Confocal images of hollow (PSS/PAH) <sub>4</sub> capsules obtained after core dissolution (FITC was added to the suspension to visualize the capsules) (a) and capsules loaded with HRP labeled with FITC (b), as well as corresponding intensity profiles across the equatorial planes of capsules.....	41
Figure 5.3: Emission and excitation spectra: (a) polymer formed in bulk solution where curve (1) represents the excitation characteristic and curve (2) represents the emission characteristic (b) excitation and emission spectra where curve (3) represents emission characteristic for polymer formed within shells (excited at 321 nm), (4) represents emission characteristic for HRP-FITC encapsulated within shells (excited at 488 nm), and (5) represents emission for empty shells (excited at 320 nm) .....	43

Figure 5.4: Confocal images of capsules with polymer formed in situ at different concentrations of monomer: a - 4 mg/ml: b – 60 mg/ml and corresponding intensity profiles. c – the same as b but additionally labeled with FITC.....	45
Figure 5.5: AFM images of capsules and height profiles of one of the capsules: (a) hollow, (b) filled with HRP, and (c) after polymerization of tyramine inside the capsule .....	46
Figure 5.6: QCM characterization showing thickness variation with deposition of each monolayer of (PSS/PDDA) <sub>4</sub> /(PSS)/(Papain/PSS) <sub>10</sub> (Papain) .....	49
Figure 5.7: QCM monitoring of change in thickness with assembly of Papain on resonator before and after polymerization. Two separate experiments were conducted with two different resonators: one for assembly of Papain and one for assembly of Papain followed by polymerization .....	50
Figure 5.8: $\zeta$ potential monitoring of assembly of (PSS/PAH) <sub>2</sub> /(PSS/Papain) <sub>3</sub> on MnCO <sub>3</sub> particles (d = 6.2 $\mu$ m) .....	51
Figure 5.9: CLSM image of MnCO <sub>3</sub> capsules with (PSS/PAH) <sub>4</sub> /(PSS/FITC-Papain) <sub>3</sub> (a) and CLSM image showing intensity variation across the equatorial plane (b).....	52
Figure 5.10: CLSM image of FITC-Papain assembled on MnCO <sub>3</sub> cores and intensity profile across equatorial plane (a), CLSM image of MnCO <sub>3</sub> cores with FITC-Papain assembled on them after polymerization with intensity profile across the equatorial plane (b) .....	53
Figure 5.11: CLSM image of MnCO <sub>3</sub> cores with FITC-Papain assembled on them after heating in DI water at 40°C for 6 hours (a), with intensity profile across the equatorial plane (b) .....	54
Figure 5.12: CLSM image of empty (Tannic Acid/Chitosan) <sub>5</sub> capsules (a) and (Tannic Acid/Chitosan) <sub>5</sub> capsules loaded with Rhodamine-labeled Papain (b) .....	55
Figure 5.13: High magnification CLSM image of empty (Tannic Acid/Chitosan) <sub>5</sub> capsule (a), CLSM intensity profile across equatorial plane of the capsule (b) .....	55
Figure 5.14: High magnification CLSM image of two (Tannic Acid/Chitosan) <sub>5</sub> capsules loaded with Rhodamine-labeled Papain (a), CLSM intensity profile across equatorial plane of a capsule (b) .....	56

## CHAPTER 1

### INTRODUCTION

#### **1.1 Multilayered Polyelectrolyte Microcapsules (PEMs)**

The past decade has witnessed significant progress in the field of nanostructured material formation. Fabrication of multilayered materials with unique properties is possible via self-assembly of polymers involving electrostatic interactions. Hong and Decher demonstrated that alternating exposure of a charged substrate to solutions of positive or negative polyelectrolytes respectively, results in a layered complex stabilized by strong electrostatic forces [1]. These self-assembled polyelectrolyte multilayers (PEMs) have proven to be versatile materials, which allow the incorporation of different charged compounds or nano-objects. Inorganic nanoparticles, functional polymers, proteins, orientable chromophores, biopolymers such as DNA, or mesogenic units inducing local order, which have been used as building blocks, are described in previous reviews [2-5].

The versatility of the multilayer formation process with respect to the variety of materials that can be used as building blocks and the possibility of combination with other assembly procedures, offers a high application potential in a broad range of different areas of materials development. Applications of planar layers include use of

matrix materials for biological sensor applications, separation membranes, and for tailored surface-modification. One of the most effective applications has been the coating of colloidal particles employing the technique of Layer-by-Layer (LbL) assembly [6]. Subsequent removal of the core leads to the formation of very stable, hollow polymeric shell structures [7]. Such hollow, thin-walled microcapsules have attracted particular interest as drug carrier systems and as “micro-reactors”. PEMs are furthermore of fundamental physical interest because of their ability to form stratified layers in two dimensions, which also can be grown step-by-step into the third dimension. This behavior, controlled by internal interfaces, differs largely from the corresponding volume material properties. The amorphous nature of PEMs in disordered systems not only determines their properties but also makes them less sensitive to the parameters of the preparation process. Theories describing PEMs today range from phenomenological descriptions of layer structure and segment distribution to mean field and scaling approaches. The structural aspects of PEMs, e.g. the dependence of layer thickness on preparation conditions, or the internal interdigitation of adjacent layers is well understood. Currently studied questions involve the presence of small ions in PEMs, local dissociation of weak polyelectrolytes in layers, and swelling behavior, i.e., the amount of water and the local hydration. Of particular interest are permeabilities of hollow capsules with respect to small ions, solvents, or macromolecules [8].

Supramolecular multicomponent nanostructures, such as ultrathin polymer films, surface-modified liposomes, and organic-inorganic composite nanosized materials, have recently gained interest in various fields of applied physical chemistry. A wide range of synthetic polyelectrolytes, biopolymers, lipids, and inorganic particles have been

successfully employed to fabricate multilayer films onto flat substrates by taking advantage of the electrostatic interaction between oppositely charged species during their stepwise adsorption from an aqueous solution [2, 9-11]. Recently, this technology has been applied to multilayer assembly on the surface of colloidal particles [12, 13]. Hollow polyelectrolyte micro and nanocapsules can be fabricated by dissolving the original templating core [13]. The encapsulation of materials within the small capsule volumes with controlled thickness, composition, and permeability of the encapsulating wall opens novel opportunities for use of these structures as “micro-reactors”, micro-carriers, and vehicles for sustained drug release formulations. According to the basic concept of the driving force of macro-ion multilayer assembly, the electrophoretic potential ( $\zeta$  potential) of colloidal particles alternates between positive and negative values at each step of the polyelectrolyte adsorption. The film thickness grows linearly with the number of layers with the thickness increase being approximately 2 nm/layer of adsorbed polyelectrolyte [14].

Permeability of the capsule wall, particularly for selectivity towards water-soluble components, could create a difference in the chemical composition between the bulk solution and the capsule interior. Mohwlad and coworkers have developed a model to study and to employ the selective permeability properties of the capsule walls to create a Donnan equilibrium situation [15]. If an electrolyte species is excluded from the encapsulated interior, the permeating counterions should be distributed on both sides of the shell wall according to the Donnan equilibrium. Their concentration would then be different on both sides of the capsule wall. In the case of protons, this condition would correspond to a pH difference. Furthermore, the presence of a non-permeating electrolyte



species in the solution on one side of the capsule wall can induce an osmotic pressure difference across the wall. This osmotic pressure difference can lead to volume changes of the hollow polyelectrolyte capsules and can affect the mechanical properties of the shell wall.

### **1.2 Enzyme Multilayers on PEMs and Enzyme Encapsulation**

Protein films are routinely employed in bioseparations, immunoassays, diagnostics, localization, and catalysis [16, 17]. Proteins have traditionally been immobilized onto solid surfaces by a variety of techniques, including physical adsorption, solvent casting, covalent binding, and electro-polymerization [16]. However, these methods often produce irregular films with a low density of protein. Ordered protein multilayer films with a high protein density have been constructed by using Langmuir-Blodgett deposition methods [16, 18] or by exploiting biospecific interactions [19, 20]. Denaturation of the immobilized proteins and the highly specific nature of the assembly process has limited the wide applicability of these methods. The process of alternating adsorption of charged macromolecules (LbL technique) offers controlled and highly ordered molecular assemblies according to a specifically designed architecture [21]. The strategy entails the stepwise adsorption of charged species onto a charged substrate, using primarily electrostatic interactions for multilayer film growth. Charge overcompensation occurs with deposition of each layer, thereby facilitating adsorption of the next layer. Multilayer films of a wide array of water-soluble proteins, alternately assembled with oppositely charged polyelectrolytes were constructed, and their successful application in catalysis [22-24] and immuno-sensing [25] was demonstrated.

Recently, a multi-filtration procedure for separation of polyelectrolyte-modified particles from unreacted polyions was introduced [26]. This procedure allows production of larger amounts of particles coated with polyelectrolytes as compared with an earlier procedure based on separation of colloids and polyions by centrifugation [27]. After the particles are coated with the desired number of polyelectrolyte layers, the core particles are dissolved to obtain empty capsules with a layer thickness tuned over a range of 5 to 50 nm and with the desired composition [26]. Shell composition and number of layers [28, 29] can vary the permeability properties of polyion capsules. It has been shown that the wall permeability for molecules of dextran and albumin depends upon pH. At low pH, the capsule walls were open, and at pH higher than 8 they were closed. By varying the pH in the capsule suspension in the presence of the macromolecules, the encapsulation was performed [30]. An operation with opening/closing capsule walls composed of polyion multilayers is based on Rubner's recent finding that varying solution pH can induce charge imbalance in polycation-polyanion complexation in the multilayer, resulting in opening of ca. 100-nm pores [31]. Formation of unique and complex colloids with tailored enzymatic activity was achieved through the assembly of polyion capsules loaded with urease [32]. In traditional bioreactors, urease was immobilized by covalent bonding or with acrylamide gel on different substrates such as glass beads, glass wool, nylon netting or nitrocellulose. Nanocomposites containing urease multilayers on 470-nm latex cores were recently prepared [33]. Encapsulation of urease in micro-shells was achieved through layer-by-layer assembly of linear polycations and polyanions on 5  $\mu\text{m}$  melamine formaldehyde (MF) cores. Sodium poly(styrenesulfonate) (PSS) and poly(allylamine) hydrochloride (PAH) were employed as polyelectrolytes for micro-shell

fabrication. After depositing the required number of layers of polyelectrolytes, the MF cores were dissolved by changing the pH to 1.1, thereby yielding hollow shells [32].

### **1.3 Enzymatic Catalysis**

Most enzymes operate at room temperature, under neutral aqueous conditions, and in the absence of substrate functional-group protection. In organic syntheses, these biocatalysts can be used as the sole catalyst in a reaction, in combination with other enzymes, or with non-biological reagents. The chiral nature of enzymes results in the formation of stereo- and region-chemically defined reaction products with significant rate acceleration (typically 10<sup>5</sup> to 10<sup>8</sup>) [34]. In addition, many enzymes accept inorganic substrates, and genetic engineering can further alter their stability, broaden their substrate specificity, and increase their specific activity. Molecules with several functional groups pose particular challenges to non-biological synthetic methods but are natural targets for biological techniques. For example, large DNA and RNA molecules can be efficiently synthesized and manipulated by enzymatic processes, whereas equivalent chemical alternatives do not exist. Using biocatalysts, otherwise impractical synthetic manipulations of complex molecules, such as carbohydrates, can be performed in an environmentally benign manner. Both natural and engineered enzymes can now be produced on a large scale in convenient host organisms using recombinant DNA technologies. The application of enzymes in synthesis thus represents a remarkable opportunity for the development of industrial chemical and pharmaceutical processes [35-37].

Recent developments in the rapidly growing field of enzymatic catalysis focus on the use of free enzymes (extracellular) in preparative asymmetric transformations. In many cases, free enzymes offer advantages over whole-cell processes, which may be more difficult to predict, control and manipulate. Over 3,000 enzymes have so far been identified, and this number may be greatly augmented in the wake of genomic and proteomic research. The enzymes that have been exploited for organic synthesis, as well as the type of reaction catalyzed, are summarized in Table 1. In general, several parameters affect the practicality of an enzymatic reaction.

**Table 1.1: Enzymes commonly used for organic syntheses**

<b>Enzymes</b>	<b>Reactions</b>
Esterase, lipases	Ester hydrolysis, formation
Amidases (proteases, acylases)	Amide hydrolysis, formation
Dehydrogenases	Oxidoreduction of alcohols and ketones
Oxidases (mono- and dioxygenases)	Oxidation
Peroxidases	Oxidation, epoxidation, halohydration
Kinases	Phosphorylation (ATP-dependent)
Aldolases, transketolases	Aldol reaction (C–C bond)
Glycosidases, glycosyltransferases	Glycosidic bond formation
Phosphorylases, phosphatases	Formation and hydrolysis of phosphate
Sulphotransferases	Formation of sulphate esters
Transaminases	Amino acid synthesis (C–N bond)
Hydrolases	Hydrolysis
Isomerases, lyases, hydratases	Isomerization, addition, elimination, replacement

The degree of inhibition by substrate or product (determined by their affinity to the enzyme) may be particularly important in the outcome of a reaction. In an ideal scenario, the enzyme used would have high specific activity and stability, and would be subject to minimal substrate and product inhibition. Furthermore, the extent of substrate specificity can determine whether a given enzyme will have general synthetic utility, with stereo-specificity being perhaps the most important parameter under consideration. Although enzymes with narrow substrate specificity are often efficient in catalyzing reactions using their natural substrate, this property becomes a limitation when the

development of catalysts for general purposes is the goal. Biocatalysts that accept a wide range of substrates to form enantiopure products are of particular interest to the synthetic chemist. Many enzymes have now proved synthetically useful and have become commercially available; however, one still cannot use enzymes for the formation of every desired linkage or resolution of any racemic mixture. Moreover, although many enzymes have been highly characterized with regard to substrate specificity and stereo-selectivity, they may be unpredictable with unnatural substrates [38].

#### **1.4 Chemical Reactions Within PEMs**

The ability to incorporate macromolecular materials within PEMs allows the use of these tiny containers as “micro-reactors”. They are particularly useful for fabrication of enzyme “micro-reactors”, when substrates and reaction products diffuse freely through the microcapsules’ walls without releasing the encapsulated enzyme. The presence of polymer molecules on only one side of the semi-permeable polyelectrolyte walls may have significant influence on reaction parameters such as pH. A pH gradient can be established across the PEM wall in different ways, depending on polybase or polyacid being inside or outside the PEMs. Physiochemical changes, such as variations in pH, have been shown to affect permeability of the PEM walls to macromolecules. The pH inside PEMs can be modulated independent of the pH of the bulk solution [15]. Semi-permeable hollow nano and micro-spheres have been employed as templates for preparation of well-defined particles of various organic and inorganic materials. Calcium carbonate ( $\text{CaCO}_3$ ) was precipitated within PEMs in presence of dextran sulfate [39]. Dextran sulfate was used to reduce super saturation and prevent bulk precipitation of  $\text{CaCO}_3$ . The properties

of the capsule interior could be changed by filling them with low molecular weight compounds and subsequent precipitation, [40] micelle formation, or solvent exchange [41] but these processes are reversible and depend on the exterior environment. For applications as “nanoreactors”, a permanent adjustment of the physicochemical properties of the interior is desirable. This result could be achieved by inclusion of macromolecules because the capsule wall is impermeable for polymers whereas monomers penetrate the wall easily. A general procedure for loading the capsules by a “ship in a bottle” synthesis was demonstrated [42]. Different polymers and functionalized copolymers have been synthesized inside the capsules from water-soluble anionic, cationic, and neutral monomers.

### **1.5 Enzyme Catalyzed Polymerization Within PEMS**

The present work describes bio-chemical synthesis of novel polymers via enzymatic catalysis within PEMS (Figure 1.1), fabricated by LbL electrostatic self-assembly. Two enzymes namely horseradish peroxidase and papain (derived from *Carica Papaya* latex), were employed as the catalytic bio-agents. Two types of template cores namely, MF and manganese carbonate ( $\text{MnCO}_3$ ), were employed for fabrication of hollow shells. The polyelectrolytes used were sodium poly (styrene sulfonate) (PSS), poly(allyl-amine hydrochloride) (PAH), tannic acid, and chitosan. Enzymatic catalysis, as discussed above, is widely applied in industrial settings as a substitute for organic synthesis [34-38]. Moreover, enzymes offer specificity to substrates making them excellent candidates for dedicated synthesis of products without the generation of unwanted by-products. In the present report, we demonstrate the ability to encapsulate

enzyme molecules and use their catalytic properties to polymerize specific substrates to form novel polymers within microcapsules. We believe this approach is unique and opens up many possibilities for synthesizing biochemical products within PEMs. Thus, PEMs can act not only as versatile and robust “reactors” that can be employed for characterization of uniform and monodispersed biopolymer particles with unique properties, but also as containers which can be modulated to effect sustained release of as-synthesized biomaterials to the environment.

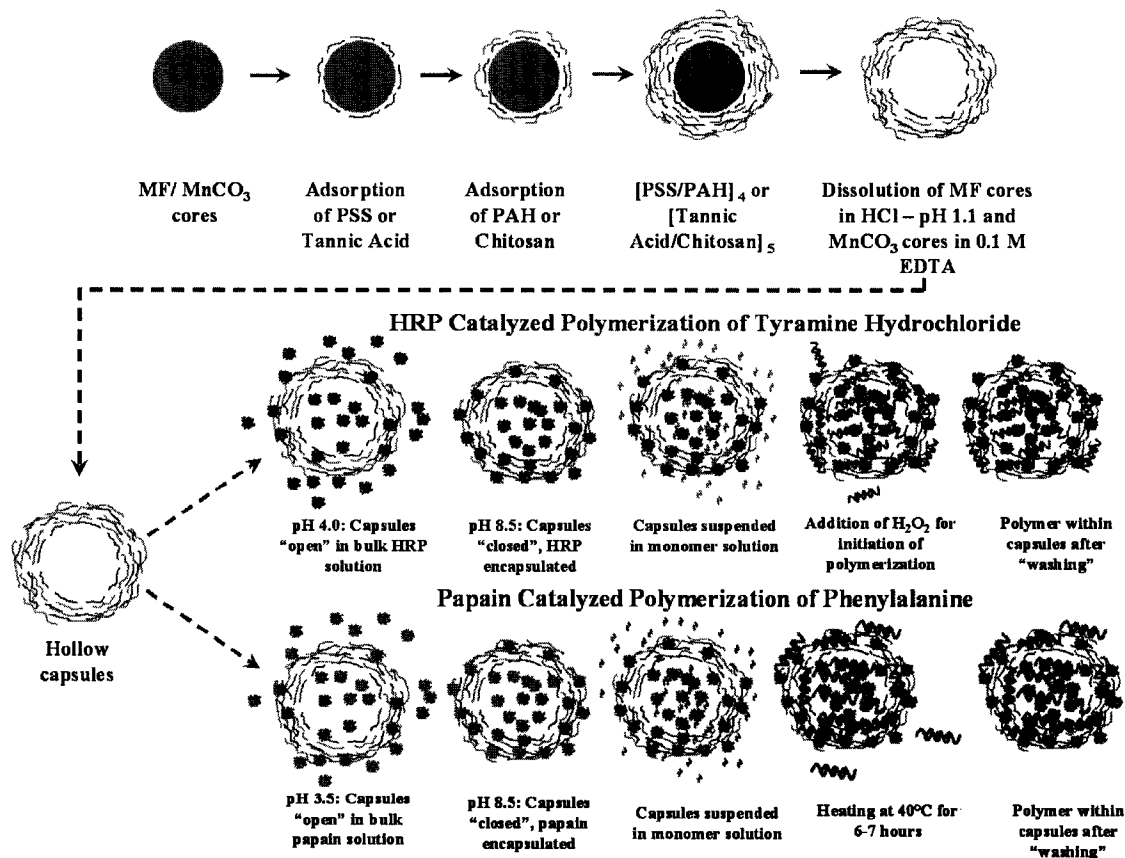


**Figure 1.1: Schematic representation of the capsule formation via LbL assembly, encapsulation of HRP and Papain within the capsules and polymer formation *in situ*.**

## **1.6 Chapter Outlines**

Following the introduction, Chapter 2 will discuss basics of enzymatic catalysis with the focus being on peroxidase and protease catalyzed polymerization reactions and their advantages. Chapter 3 will outline the materials employed in experimentation in the present study and the methodologies on which experimentation was based. Chapter 4 will briefly discuss the different instruments used for characterization and their respective working-principle. Chapter 5 is a detailed discussion of the results obtained from experimentation, which include polymerization catalyzed by horseradish peroxidase and polypeptide synthesis catalyzed by papain. Chapter 6 concludes the report with recommendations for future work that can be continued based on the present results. Chapter 6 is followed by a complete list of references consulted for writing this report.



## CHAPTER 2

### ENZYME-CATALYZED SYNTHESIS

#### 2.1 Historical Perspective on Enzymatic Catalysis

Much has been written about the historical exploration of enzymatic catalysis. Among the first hypotheses offered is the "lock and key" model [43], which proposed that the binding of a substrate molecule to the active site on the enzyme results in activation of the substrate (reactive conformation). A modified version proposed that the "key does not quite fit the lock perfectly but exercises a certain strain on it" (ground-state destabilization) [44]. With the advent of transition-state theory, the hypothesis of enzyme-transition-state complementarity [45], which discovered a preferential binding of the transition state rather than the substrate or product as the source of catalysis, gained prominence. The comparison between enzyme-catalyzed and noncatalytic rates has provided an estimate of the degree of stabilization of the enzymatic transition-state. Careful measurements of the rates for spontaneous hydrolysis of ionized phosphate monoesters and diesters relative to *Escherichia coli* alkaline phosphatase [46] or staphylococcal nuclease acting on the same substrate reveals that these enzymes enhance the rate of the hydrolysis reaction.

It has been proposed that catalysis, which takes advantage of thermodynamic state function descriptors of the free energy of activation [47] for the substrate and transition states, the catalytic power of enzymes will always be evident as a result of increased transition-state stabilization (lower free energy) for processes relative to the reference reaction. There has been an increased scrutiny of how the binding interactions arising from favorable and unfavorable non-covalent bonding between the reactants and residues within the active site are translated into catalysis [48, 49]. Parallel with the ability to see the x-ray crystallographic structures of enzymes was the advent of numerous physical organic studies on various model systems that mimicked active-site features [50]. The details of general acid-base and nucleophilic catalysis for acyl-transfer reactions and glycoside and acetal hydrolysis highlighted the possibility of stepwise or concerted proton transfers to and from meta-stable intermediates or transition states with chemical entities such as amines, imidazoles, and carboxylates, which function in the active site. These studies [51, 52] provided fresh insight into the chemical identity of species along the reaction coordinate that links ground and transition states. Similarly, physical organic experiments in which a given chemical reaction was performed in various solvents, generally ranging from aprotic to protic, showed that the effect of the solvent is to retard the rate relative to what would be observed for this reaction under the same conditions in the gas phase. Alternatively, the effect may be described as solvent substitution, with the active-site residues furnishing a polar framework to replace the solvating water molecules [53].

## **2.2 Enzyme Catalyzed Polymerization**

Enzyme-catalyzed polymerization, in particular, has been receiving attention from the viewpoint of environmental issues because reaction proceeds under mild conditions [54]. In this environmental-benign polymerization, several enzymes, such as oxydo-reductase (lipase, horseradish peroxidase and so on.), catalyze the polymer synthesis reaction. All the naturally occurring polymers are produced *in vivo* by enzymatic catalysis. Polymerizations of substituted phenols [54-59], lacton [60-61], aromatic amines [62] have been investigated using various enzymes as a new route for polymer synthesis. Reports dealing with the *in vitro* synthesis not only of biopolymers but also of non-natural synthetic polymers through enzymatic catalysis have been published [63-72]. These enzyme-catalyzed polymerizations are gaining importance to satisfy the increasing demands in the production of various functional polymers in material science. Main target macromolecules for the enzymatic polymerization are polysaccharides, polyesters, poly(amino) acids, and polyaromatics. The first three classes of polymers can be synthesized using hydrolases as the catalyst. Hydrolases are enzymes which catalyze the hydrolysis of polysaccharides, fats (triglycerides), or peptides. However, by selecting the reaction conditions, they can also act as catalysts of the reverse reaction, leading to polymer formation. Polyaromatics, polyphenols, and polyanilines are synthesized by an enzymatic oxidative coupling. Phenol-formaldehyde resins using pre-polymers such as novolaks and resols are widely used in industrial fields [73]. These resins show excellent toughness and temperature-resistant properties, but the general concern over the toxicity of formaldehyde has resulted in limitations on their preparation and use. Therefore, an alternative process for the synthesis of phenolic polymers avoiding the use of

formaldehyde is strongly desired. Mimicking nature, the enzymatic synthesis of polyphenols has been extensively investigated in the last decades [74-77], where various oxido-reductases play an important role in maintaining the metabolism of living systems.

### **2.3 Peroxidase Catalyzed Polymerization**

So far, several enzymes of this class (peroxidase, laccase, bilirubin oxidase, etc.) have been reported to catalyze the oxidative polymerization of phenol derivatives, and among them, peroxidases are the biocatalysts most often used. Peroxidases are enzymes that catalyze the oxidation of a suitable donor by action of hydrogen peroxide, liberating two water molecules. Horseradish peroxidase (HRP) is a single-chain *b*-type hemoprotein that catalyzes the decomposition of hydrogen peroxide at the expense of aromatic proton donors. HRP has a Fe-containing porphyrin-type structure and is well known to catalyze coupling of a number of phenol and aniline derivatives using hydrogen peroxide as oxidant. Peroxidase-catalyzed oxidative coupling of phenols proceeds fast in aqueous solutions, giving rise to the formation of oligomeric compounds. However, the resulting oligomers have not been well characterized because most of them show low solubility towards common organic solvents and water. In 1987, enzymatic synthesis of a new class of polyphenols was first reported. An oxidative polymerization of *p*-phenylphenol using HRP as catalyst was carried out in a mixture of water and water-miscible solvents such as 1, 4- dioxane, acetone, *N, N*-dimethylformamide (DMF), and methyl formate [78]. The polymerization proceeded at room temperature. During this process, powdery polymers were precipitated. The reaction medium composition greatly affected the molecular

weight, and the polymer with the highest molecular weight ( $2.6 \times 10^4$  Da) was obtained in 85 % v/v 1,4-dioxane.

Phenol, the simplest and industrially most important phenolic compound, is a multifunctional monomer when considered to be used as a substrate for oxidative polymerizations, and hence conventional polymerization catalysts afford insoluble macromolecular products with non-controlled structures [79]. Phenol was subjected to the oxidative polymerization using HRP or soybean peroxidase (SBP) as a catalyst in an aqueous dioxane mixture, yielding a polyphenol consisting of phenylene and oxy-phenylene units (Figure 1). The resulting polymer showed low solubility; it was partly soluble in DMF and dimethyl sulfoxide (DMSO), and insoluble in other common organic solvents [80, 81].

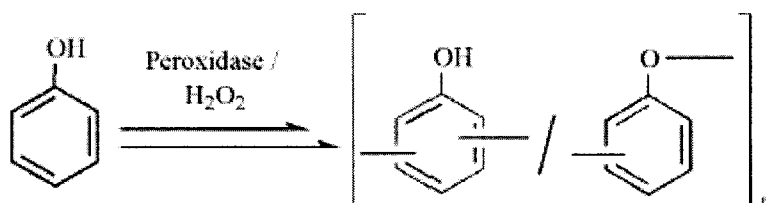


**Figure 2.1: Oxidative polymerization of phenol catalyzed by HRP in aqueous dioxane mixture yielding phenylene and oxy-phenylene units**

Combination of enzyme-catalyzed syntheses with the engineering of micro- and nanoparticles and shells to add new properties is of special interest because of its bio- and environmental compatibility and efficiency [82-88]. Application of LbL assembly to tiny soluble cores allows the formation of microcapsules [89]. Encapsulation of proteins within polyelectrolyte multilayers or inside hollow polyelectrolyte capsules has been recently demonstrated [89-93]. A number of proteins have been encapsulated in such

micro-shells, and their retained activity has been proven [91-94]. Possible applications of these microcapsule reactors for organic or inorganic synthesis in a confined volume are now being investigated [95]. Controllable polymer synthesis on the surfaces of such micro-capsules has been demonstrated by combining two approaches: first, LbL assembly of linear polyelectrolytes and enzymes to produce microcapsules with nano-organized walls and second, producing a phenol polymer coating on the surface of such microcapsules. Peroxidase-catalyzed polymerization of phenols and anilines has proven to be an efficient tool for the production of a polymer, with specially designed properties, inside of the polyion microcapsules and onto their outermost surface [96]. Horseradish peroxidase is an enzyme commonly used in immuno- and protein activity assays [97]. Among the substrates for peroxidase, several water-soluble phenols produce polymeric fluorescent products [98-100]. The monomers can be modified by introducing different side groups for specific applications including selective binding of organic ligands and drugs [84-85]. The catalytic cycle for horseradish peroxidase is well studied. The enzyme passes through three oxidation states following its reaction with hydrogen peroxide and subsequent reaction with an aromatic substrate [99-102]. Products of this cycle are water and highly reactive free radicals. These radicals then undergo coupling to produce dimers. Successive oxidation, coupling and a transfer reaction eventually result in the formation of the polymer. The generation of radicals in this cycle is enzyme dependent. However, radical-radical coupling and transfer are controlled exclusively by phenoxy radicals and solvent chemistry [101-102]. Tyrosine moieties in peroxidase seem to be the binding sites for forming polymeric chains.

## **2.4 Protease Catalyzed Polymerization**

Despite the fact that well-established approaches to synthetic peptide chemistry have been successful in making peptides and small proteins of biological and pharmaceutical interest, synthetic methodology continues to develop innovative strategies based on suitable peptide ligases. A universally applicable peptide ligase, which principally would display high catalytic efficiency for all possible combinations of amino acids to be coupled, would justify full use of enzymatic alternatives [103]. The ideal tool would be a nonspecific peptide ligase, as represented by the ribosomal peptidyl transferase. Unfortunately, the latter is a ribozyme [104], unsuitable for simple practical use as a catalyst outside the ribosome. Bergmann and Fraenkel-Conrat [105] confirmed Van't Hoff's prediction in 1898 that the reverse potential of proteases could be used as catalysts for peptide bond formation by characterizing simple model reactions. Because of their stereo-selectivity and mild reaction conditions, proteases (in particular serine and cysteine proteases) have been used over the last decades to complement chemical coupling methods and allow even small proteins to be synthesized by block-wise enzymatic coupling of synthetic fragments [106-110]. Currently, important large-scale industrial processes involving the enzymatic approach are the production of aspartame and human insulin.

Biodegradable polymeric materials are becoming increasingly important from the viewpoint of waste-disposal problems associated with petroleum-based plastics [111]. Poly(amino acid)s are biodegradable and can be employed for medical, cosmetic, and fabric materials [112]. Poly ( $\alpha$ -amino acid)s with high molecular weight are readily

synthesized by ring-opening polymerization of  $\alpha$ - amino acid N-carboxylic anhydrides (NCAs). However, toxic phosgene derivatives are employed for monomer synthesis [113]. It is generally accepted that an enzymatic reaction is virtually reversible, and hence, the equilibrium can be controlled by appropriately selecting the reaction conditions. Based on this view, many of the hydrolases, which are enzymes that catalyze bond-cleavage by hydrolysis, have been employed as catalysts for the reverse reaction of bond-formation [114].

Enzymatic peptide synthesis, that is catalyzed by aspartyl proteinases is controlled by multiple factors, among which enzyme specificity plays a prominent role. Thus pepsin (115, 116) and its homologue, chymosin (117), preferentially catalyze the formation of the peptide bonds between two hydrophobic amino acid residues which agrees fairly well with the data on the specificity of these enzymes, as revealed by hydrolysis of protein substrates (118,119). Occasionally, however, the bonds not corresponding to the commonly accepted enzyme preferences, e.g. phenylalanine-arginine (116), were also formed efficiently in the presence of pepsin or chymosin. This phenomenon indicates that the reaction rate, a parameter primarily taken into consideration when the enzyme specificity is to be defined appears to be less important than other limiting factors, e.g. the equilibrium position or the enzyme inhibition by the reactants. A large excess of the enzyme introduced into the reaction mixture and the duration of the synthesis process often allow the negative impact of imperfect substrate binding to be surpassed. Since such an effective broadening of the enzyme specificity markedly enhances its application range, porcine pepsin was tested as a method to overcome the specificity limitations. The capacity of pepsin to catalyze the formation of the peptide bonds was tested. Among the



bonds, were those formed by hydrophilic amino acid residue, non-protein amino acids and amino acid derivatives substituted in their side chains. For comparison purposes, several peptides were prepared that contain tyrosine, tryptophan and other amino acids, which comply with pepsin subsite-specificity requirements [120].

## CHAPTER 3

### MATERIALS AND METHODS

#### 3.1 Materials

Poly (sodium 4-styrene sulfonate) (PSS, MW 70 000) and poly(allylamine hydrochloride) (PAH, MW 70,000) were purchased from Aldrich. Peroxidase from Horseradish (HRP, 250-330 units/mg solid), fluorescein isothiocyanate (FITC) and FITC labeled peroxidase (HRP-FITC, 200 units/mg solid), hydrogen peroxide (H<sub>2</sub>O<sub>2</sub>, 35 wt %), hydrochloric acid (HCl, 36 wt %), 4-(2-aminoethyl) phenol hydrochloride (tyramine) were obtained from Sigma. Monodisperse particles (diameter  $\sim 5.06 \pm 0.16 \mu\text{m}$ ) of weakly polymerized melamine formaldehyde (MF) were obtained as a 10 % solution in DI water from Microparticle GmbH, Germany. (PAH, MW 50,000), MnSO<sub>4</sub>, NH<sub>4</sub>HCO<sub>3</sub> and NaCl were obtained from Aldrich. Papain (from *Carica Papaya* latex), phenylalanine, and glutamic acid were obtained as a gift from Polytechnic University, NY, courtesy Dr. Richard Gross, and were used as received. Tannic acid (TA, 90 % penta-m-digalloyl glucose, Sigma-Aldrich), chitosan (CHW, medium viscosity, Wako) were used as received. Structural formulae for PSS, PAH, phenylalanine, glutamic acid, tannic acid, and chitosan are shown in Figures 3.1, 3.2, 3.3, 3.4, 3.5, and 3.6 respectively.

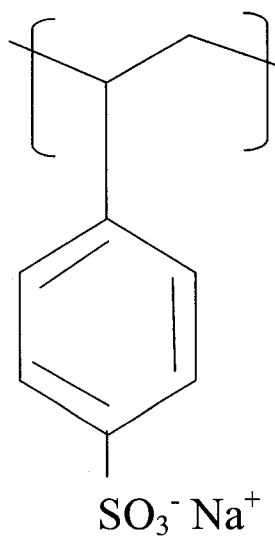


**Figure 3.1: Structural formula for PSS**

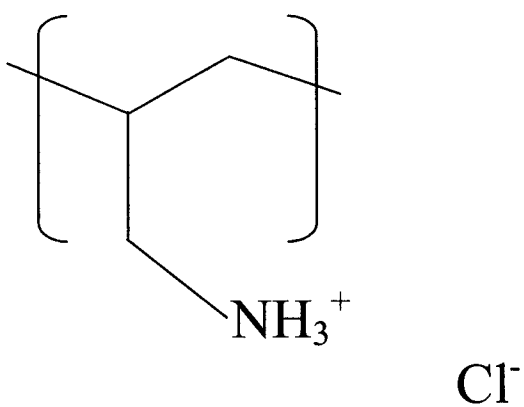


**Figure 3.2: Structural formula for PAH**

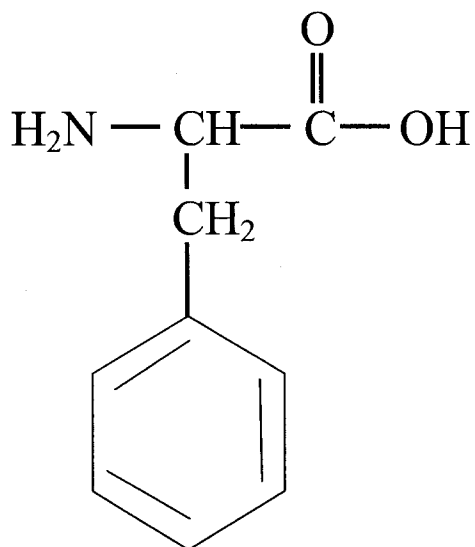


**Figure 3.3: Structural formula for Phenylalanine**

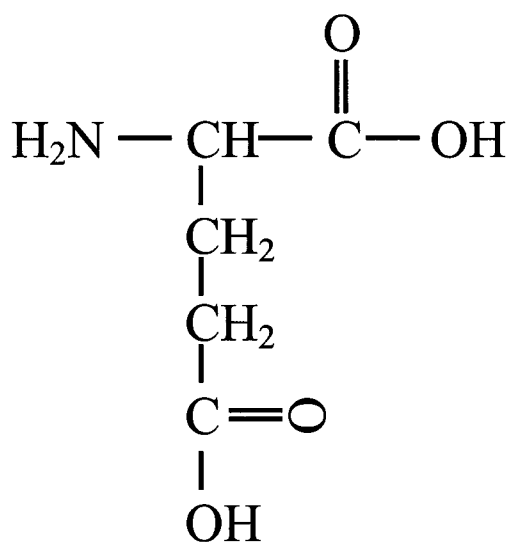


**Figure 3.4: Structural formula for Glutamic acid**

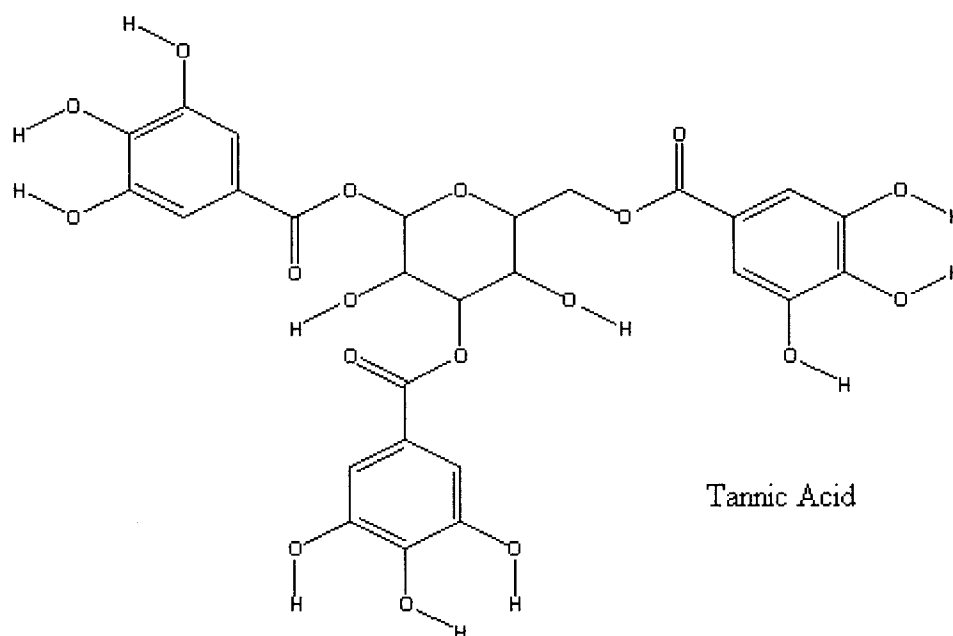


**Figure 3.5: Structural formula for Tannic acid**

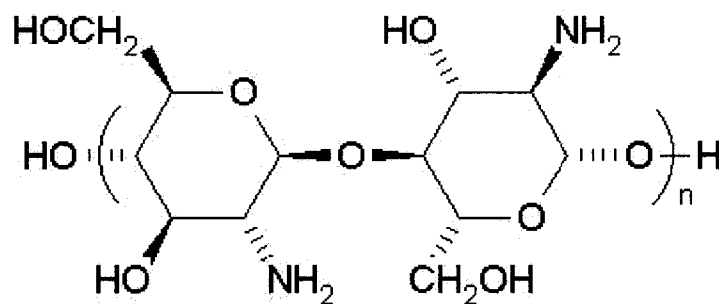


**Figure 3.6: Structural formula for Chitosan**

### 3.2 $\text{MnCO}_3$ Template Particle Formation

The manganese carbonate template was prepared by a simple mixing method described in reference [121]: Acidic manganese sulfate solution ( $9 \times 10^{-3}$  M, pH = 4.2 adjusted with sulfuric acid) was added in a one-to-one volume ratio to  $2.25 \times 10^{-3}$  M

$\text{NH}_4\text{HCO}_3$ . The stirred mixture was then aged at  $50^\circ\text{C}$  for 16 h. The resulting  $\text{MnCO}_3$  particles had a round shape with a diameter of 4-6  $\mu\text{m}$ .

### **3.3 Preparation of (PSS/PAH)<sub>4</sub> Microcapsules**

Deposition of polyelectrolyte multilayers on MF cores was accomplished using the procedure reported elsewhere [122]. Typically, PAH and PSS solutions (0.2 mL of 3 mg/mL in 0.5 M NaCl) were alternately added to 1.5 mL of core suspension. This addition resulted in dilution of suspension of MF particles to 1% at pH 6.5. Each polyelectrolyte layer was adsorbed for 15 min, and then three intermediate washings with deionized (DI) water were made, before the addition of the next layer to remove polyelectrolytes remaining in supernatant solution. The assembly of the layers on MF cores was confirmed by monitoring alternating changes of electrophoretic potential ( $\zeta$  potential) after deposition of every layer using a Brookhaven Instruments Corp. zeta potential analyzer. For the measurement, 20  $\mu\text{L}$  of the sample was diluted to 1.5 mL with DI water. After deposition of eight alternate polyelectrolyte layers, the MF cores were dissolved by treatment with HCl (pH < 1.0). The capsules obtained were washed with DI water until the capsule suspension was stabilized at pH 5.5. For negatively charged  $\text{MnCO}_3$  template particles the layer-by-layer assembly procedure was the same except starting from the first PAH layer. In all cases, the polyelectrolyte concentration was much larger than would be required for saturation coverage of the particles. After deposition of four bilayers of (PSS /PAH)<sub>4</sub>, the template core was dissolved by treatment with 0.1 M EDTA solution for 3-4 hours. Hollow polyelectrolyte capsules were obtained.

### **3.4 Encapsulation of HRP in Microcapsules**

A (PSS/PAH)<sub>4</sub> capsules suspension, volume 200  $\mu$ L, was mixed with 200  $\mu$ L of HRP solution (3 mg/mL, pH 4.0), and the mixture was kept at room temperature for 24 h. Horseradish peroxidase is stable under these conditions [123, 124]. As the next step, the pH of the mixture was adjusted to 8.5, and after 1 h, three washing-centrifugation cycles were carried out to remove the residual peroxidase that was not encapsulated. Confocal microscopy (a Leica DMRE2, Germany) was used to verify encapsulation of FITC-labeled peroxidase.

### **3.5 Polymerization Catalyzed by HRP**

Equal volumes (200  $\mu$ L) of the suspension of capsules with HRP encapsulated within and tyramine (4-60 mg/mL) solutions were mixed at pH 8.5. After 1 h, the polymerization was started by the addition of hydrogen peroxide to a final concentration of 0.2 M. The reaction mixture was kept for 24 h at 25°C. Traces of monomer and polymeric chains with relatively low molecular weight were then removed by washing with DI water. The masses of hollow capsules with peroxidase and polymer synthesized within were estimated according to the procedure reported [125-128]. The mass of dry capsules suspended in a predetermined volume of DI water, was determined by QCM weighing, and an amount of them in 1 mL was calculated from confocal laser scanning microscopy images using the transmission mode. A sample of free polymer in solution was prepared by mixing 400  $\mu$ L of tyramine (3 mg/mL), 100  $\mu$ L of HRP (3 mg/mL), and 10  $\mu$ L of hydrogen peroxide (35 wt %) at pH 8.5 in order to compare the properties of polymer formed within microcapsules and that in free solution.

### **3.6 Preparation of [Tannic acid (TA)/Chitosan (CHW)]<sub>4-5</sub> Hollow Capsules**

Four and five bilayer (TA/CHW)<sub>4-5</sub> capsules were deposited on MnCO<sub>3</sub> cores with a diameter of 4.0 μm ± 0.2 μm prepared according to the procedure reported [122]. Typically, 0.4 mL of 1 mg/mL TA or chitosan solution (pH 5.0) was added alternatively to 2 mL of the suspension containing 10 mg of the cores. After allowing 15 min for deposition of each layer, the particles were washed with DI water three times using centrifugation protocol. The assembly was monitored with ζ potential measurements using a *Brookhaven Zeta Plus* micro-electrophoretic instrument. For dissolution of MnCO<sub>3</sub> cores, the resulting particles were re-suspended in 2 mL of a 0.1 M EDTA solution at pH 5.0. After 4 days at room temperature, the supernatant was replaced with a new portion of EDTA solution for an additional 12 hours. Finally, the capsules were rinsed three times with DI water. Atomic Force Microscopy (AFM) images of dried capsules on mica were taken on a *Q-Scope<sup>TM</sup> 250 Quesant* instrument in intermittent-contact mode. Confocal Laser Scanning Microscopy was used to analyze the structure of the obtained microcapsules.

### **3.7 LbL Self Assembly of Papain on QCM Resonator and MnCO<sub>3</sub> Cores**

The LbL assembly by alternate adsorption of polyions and papain was carried out by immersion of QCM resonators in appropriate solutions for 20 min. Three intermediate washings were performed after each layer by gentle agitation in water followed by drying



in a nitrogen stream. At the first step of the assembly, a positively charged surface was formed by adsorption of cationic PAH. A USI System, Japan, QCM instrument was used to monitor the assembly. Only silver electrode QCM resonators were used in the study. The precursor of (PSS/PAH) $_n$  ( $n = 3, 4$ ) was deposited on each resonator followed by deposition of 5 bilayers of (PSS/Papain). From the corresponding QCM frequency shift, thicknesses of individual layers were estimated using the formula [129]

$$\Delta D = -0.016 \cdot \Delta F \text{ (Hz)}.$$

For assembly of papain on MnCO<sub>3</sub> cores, PAH and PSS solutions (0.2 mL of 3 mg/mL in 0.5 M NaCl) were alternately added to 1.5 mL diluted to 1% suspension of MnCO<sub>3</sub> cores at a pH 6.5. Each polyelectrolyte layer was adsorbed for 15 min, followed by three intermediate washings with deionized (DI) water, before addition of the next layer, to remove any polyelectrolytes remaining in the supernatant solution. The assembly of the layers on MnCO<sub>3</sub> cores was confirmed by monitoring alternate changes of  $\zeta$  potential using a Brookhaven Instruments Corp. zeta potential analyzer. The assembly sequence followed was [(PSS/PAH) $_4$ / (PSS/Papain) $_{4-5}$ ]. Papain was always assembled as the outermost layer.

### **3.8 Polymerization Catalyzed by Papain on MnCO<sub>3</sub> Cores**

Equal volumes (200  $\mu$ L) of the suspension of MnCO<sub>3</sub> cores with [(PSS/PAH) $_4$ / (PSS/Papain) $_{4-5}$ ] and phenylalanine (120 mg/mL) solutions were mixed at pH 8.5. The reaction mixture was kept in a water bath at 40°C with constant stirring for 5-6 hours. Traces of monomer and polymeric chains with relatively low molecular weight were removed by washing with DI water. Confocal Laser Scanning Microscopy was used to

analyze the structure of the  $\text{MnCO}_3$  cores with [(PSS/PAH)<sub>4</sub>/ (PSS/Papain)<sub>4-5</sub>] after polymerization. As a control,  $\text{MnCO}_3$  cores with [(PSS/PAH)<sub>4</sub>/ (PSS/Papain)<sub>4-5</sub>] were heated without addition of phenylalanine (monomer) at 40°C with constant stirring for 5-6 hours.

### **3.9 Encapsulation of Papain in (TA/CHW)<sub>5</sub> Microcapsules**

(TA/CHW)<sub>4-5</sub> capsules in suspension (pH 5.0), volume 300  $\mu\text{L}$ , was mixed with 300  $\mu\text{L}$  of Rhodamine-labeled Papain solution (3 mg/mL, pH 5.0), and the mixture was kept at room temperature for 24 h. Papain is stable under these conditions [130]. As the next step, the pH of the mixture was adjusted to 8.5, and after 2 h, three washing-centrifugation cycles were carried out to remove the residual papain that was not encapsulated. Confocal microscopy was used to verify encapsulation of Rhodamine-labeled papain.

### **3.10 Characterization of Capsules**

The size, integrity, and loading amount of the enzyme and polymer into a capsule was characterized using a confocal microscope. The loading was estimated as  $((F_{\min} - F_0)/(F_{\max} - F_0)) \times 100\%$ , where  $F_{\max}$ ,  $F_{\min}$ , and  $F_0$  are the intensities of the signal from the walls and interior of the capsule and from outside the capsule obtained from a profile of fluorescence along the capsule cross section. Fluorescently labeled peroxidase (HRP-FITC) and (FITC-Papain) was used to visualize the distribution of the encapsulated protein. For visualization of morphology and distribution of polymer within a capsule

FITC was added to the capsule suspension. When non-labeled peroxidase (HRP) was used, the polymer of tyramine that is formed in situ, is the only product which exhibits fluorescence. The emission and excitation characteristics of the polymer formed in solution and inside the capsules were studied using a fluorescence spectrometer (Photon Technology International Inc.). Although the intensity of polymer fluorescence for excitation-emission conditions available with the confocal microscope was rather weak, it was sufficient to confirm the formation of the polymer and to characterize its distribution within the capsule interior. The atomic force microscopy (AFM) images of hollow capsules, capsules filled with peroxidase, and those after polymerization of tyramine within the capsules were obtained using a Q-Scope 250 Quesant instrument with intermittent-contact mode. Samples for AFM were prepared by applying 5  $\mu\text{L}$  of capsule suspension on a fresh cleaved mica surface followed by drying of the samples in air, at room temperature.

## CHAPTER 4

### INSTRUMENTATION

#### 4.1 QCM characterization

QCM was used to characterize the growth of protein and polyelectrolyte layers using the principle of frequency change with change in mass of the QCM resonator used as a substrate for deposition.

The QCM uses the piezoelectric properties of quartz crystal. An electric field is applied to gold or silver coated crystals, which causes a shear deformation (parallel to the surface). The crystal can be made to resonate if an alternating field is applied at a particular frequency. This resonant frequency is given by an empirical equation (equation 4.1) [131].

$$f_0(m) = \frac{\sqrt{\mu_q}}{2x_q \sqrt{\rho_q}}$$

**Equation 4. 1**

where

$\mu_q$  = shear modulus of the quartz crystal ( $2.947 \times 10^{11}$  dyne/cm<sup>2</sup> for AT--cut quartz crystal)

$\rho_q$  = density of quartz ( $2.648 \text{ gm cm}^{-3}$ )

$x_q$  = thickness of the quartz

The deposition of gold or silver to form the electrodes dampens the resonant frequency. However, the deposition of nanoparticle monolayers further dampens this frequency. The relation between the dampening of frequency to the change in the surface attached mass, assuming a thin uniform rigidly attached mass, is given by the Sauerbrey equation (equation 4.2) [132], derived in the following sequence:

$$M = \frac{m}{A} = x_q \rho_q$$

**Equation 4. 2**

where

M = mass of the quartz crystal per unit area

m = total mass of the quartz crystal

A = area of the quartz crystal

The equation 4.2 can be combined with equation 4.3 to give

$$f_o(M) = \frac{\sqrt{\mu_q \rho_q}}{2(M)}$$

**Equation 4. 3**

The addition of mass (per unit area)  $\Delta M$  causes a change in resonant frequency  $\Delta f_o$

yields

$$f_o(M) + \Delta f_o = \frac{\sqrt{\mu_q \rho_q}}{2(M + \Delta M)}$$

**Equation 4. 4**

Combining above two equations, we get

$$\Delta f_0 = \frac{\sqrt{\mu_q \rho_q}}{2(M + \Delta M)} - \frac{\sqrt{\mu_q \rho_q}}{2M}$$

**Equation 4. 5**

$$= -\frac{\sqrt{\mu_q \rho_q} \Delta M}{2(M + \Delta M)M}$$

**Equation 4. 6**

$$= \frac{-\sqrt{\mu_q \rho_q} \Delta M}{2M^2 \left(1 + \frac{\Delta M}{M}\right)}$$

**Equation 4. 7**

Combining equation 4.7 with the equation 4.3, we get

$$\Delta f_0 = \frac{-f_0(M) \Delta M}{M \left(1 + \frac{\Delta M}{M}\right)}$$

**Equation 4. 8**

For a very small mass deposited, where  $\Delta M \ll M$  equation 4.8 when combined with equation 4.2 becomes

$$\Delta f_0 = \frac{-f_0(0)\Delta M}{M} = \frac{-f_0(0)\Delta m}{Ax_q\rho_q}$$

**Equation 4. 9**

where  $f_0(0)$  is the resonant frequency (with no attached mass)

Thus the Sauerbrey equation is given as

$$\Delta f_0 = -\left\{ \frac{f_0(0)}{Ax_q\rho_q} \right\} \Delta m = -S\Delta m$$

**Equation 4. 10**

where

$\Delta m$  = the change in surface mass

A = piezoelectrically active area

S = Sauerbrey constant

The Sauerbrey constant is independent of any solution chemistry as the constant depends on well-defined physical constants. Therefore, no calibration is required for the instrument, which uses the Sauerbrey equation to calculate mass data).

For the experiments carried out in this work, the version of Sauerbrey equation used is

$$\Delta F(Hz) = -0.87\Delta M(ng)$$

**Equation 4. 11**

The equation for calculating the thickness of the deposited films is

$$\Delta t(nm) = \frac{\Delta M(ng)}{A\rho}$$

**Equation 4. 12**

## **4.2 “Zeta-Plus” Potential Measurement**

Particles dispersed in liquids usually have a charge on their surfaces. If an electric field is applied in the liquid, these particles will move towards the positive or negative pole of the field applied, depending on their charge. The sign and magnitude of the zeta potential indicated by the zeta potential measurement instrument characterizes the surface properties of materials. These parameters are a function of pH, surfactant, salt, or dispersing agent concentration. The repulsive forces in electrostatically stabilized systems are determined by the zeta potential measurement instrument and therefore are a measure of changes in relative stability. High values, either positive or negative, signify stability whereas values approaching zero signify instability, typically either flocculation or coagulation. The charge, which develops at the interface between a colloidal particle and the liquid medium in which it is suspended, may arise by any of several mechanisms. Among these are the dissociation of ionogenic groups in the particle surface and the differential adsorption from solution of ions of different charges into the surface region; in clays, ion exchange mechanisms may also be important. The development of a net charge at the particle surface affects the distribution of ions in the neighboring interfacial region, resulting in an increased concentration of counter-ions of charge opposite to that of the particle close to the surface, which results in an electrical double layer at the particle--liquid interface. This double layer may be considered to consist of two parts: an



inner region, which includes ions bound relatively strongly to the surface (including specifically adsorbed ions), and an outer, or diffuse, region in which the ion distribution is determined by a balance of electrostatic forces and random thermal motion. The potential in this region therefore decays as the distance from the surface increases until, at sufficient distance, it reaches the bulk solution value, conventionally taken to be zero.

When the sample is subjected to an electric field as in microelectrophoresis, each particle and its most closely associated ions move through the solution as a unit and the potential at the boundary between this unit, i.e., at the surface of shear between the particle with its ions and the surrounding medium, is known as the zeta potential. Zeta potential is therefore a function of the surface charge of the particle, any adsorbed layer at the interface and the nature and composition of the surrounding medium in which the particle is suspended. It is usually of the same sign as the potential actually at the particle surface [133].

### **4.3 Confocal Laser Scanning Microscope (CLSM)**

Confocal Microscopy (also referred to as CSLM, Confocal Scanning Laser Microscopy) is now established as a valuable tool for obtaining high-resolution images and 3-D reconstructions of a variety of specimens. In CLSM, a laser light beam is expanded to make optimal use of the optics in the objective. Through an x-y deflection mechanism this beam is turned into a scanning beam, focused to a small spot by an objective lens onto a fluorescent specimen. The mixture of reflected light and emitted fluorescent light is captured by the same objective and (after conversion into a static

beam by the x-y scanner device) is focused onto a photo detector (photomultiplier) via a dichroic mirror (beam splitter). The reflected light is diverted by the dichroic mirror while the emitted fluorescent light passes through in the direction of the photomultiplier. A confocal aperture (pinhole) is placed in front of the photo detector, such that the fluorescent light (not the reflected light) from points on the specimen that are not within the focal plane where the laser beam was focused (the so-called out-of-focus light) will be largely obstructed by the pinhole. In this way, out-of-focus information (both above and below the focal plane) is greatly reduced. This becomes especially important when dealing with thick specimens. The spot that is focused on the center of the pinhole is often referred to as the "confocal spot" [134]

A 2-D image of a small partial volume of the specimen centered on the focal plane (referred to as an optical section) is generated by performing a raster sweep of the specimen at that focal plane. As the laser scans across the specimen, the analog light signal, detected by the photomultiplier, is converted into a digital signal, contributing to a pixel-based image displayed on a computer monitor attached to the LSCM. The relative intensity of the fluorescent light, emitted from the laser-hit point, corresponds to the intensity of the resulting pixel in the image (typically 8-bit grayscale). The plane of focus (Z-plane) is selected by a computer-controlled fine-stepping motor, which moves the microscope stage up and down. Typical focus motors can adjust the focal plane in increments as small as 0.1 micron. A 3-D reconstruction of a specimen can be generated by stacking 2-D optical sections collected in series [135]. For characterization, a 5mL sample was placed on a microscope slide. A drop of oil was applied to the bottom of the microscope slide when using the "oil-objective" (64X). After focusing the sample

manually, LEICA software integrated with the CLSM aided in the visualization and characterization of the sample.

#### **4.4 Fluorescence Spectrophotometer (FS)**

Fluorescence occurs when a molecule absorbs light photons from the ultraviolet (UV) to visible light spectrum, (known as excitation) and then rapidly emits light photons as it returns to its ground state. Fluorimetry characterizes the relationship between absorbed and emitted photons at specified wavelengths. All chemical compounds absorb energy which causes excitation of electrons bound in the molecule, such as increased vibrational energy or, under appropriate conditions, transitions between discrete electronic energy states. For a transition to occur, the absorbed energy must be equivalent to the difference between the initial electronic state and a high-energy state. This is termed the excitation wavelength. If conditions permit, an excited molecule will return to ground state by emission of energy through heat and/or emission of energy quanta such as photons. The emission energy or wavelength of these quanta are also equivalent to the difference between two discrete energy states and are characteristic of the molecular structure. Fluorescence occurs when a molecule absorbs photons from the UV-visible light spectrum (200-900 nm), causing transition to a high-energy electronic state and then emits photons as it returns to its initial state in less than  $10^{-9}$  sec. Some energy within the molecule is lost through heat or vibration so that emitted energy is less than the exciting energy; i.e., the emission wavelength is always longer than the excitation wavelength. The difference between the excitation and emission wavelengths is called the Stokes shift

[136]. Fluorescence excitation and emission characteristics were recorded with a Fluorescence Spectrophotometer.

#### **4.5 Atomic Force Microscope (AFM)**

The atomic force microscope is one of about two dozen types of scanned-proximity probe microscopes. All these microscopes work by measuring a local property, such as height, optical absorption, or magnetism, with a probe or "tip" placed in close proximity to the sample. The small probe to sample separation (approximately the instrument's resolution) makes it possible to take measurements over a small area. The resulting image resembles an image on a television screen in that both consist of many equally spaced rows or lines of information. Unlike traditional microscopes, scanned-probe systems do not use lenses. The size of the probe, rather than diffraction effects, generally limits resolution. The AFM operates by measuring attractive or repulsive forces between a tip and the sample [137]. In its repulsive "contact" mode, the instrument lightly touches a tip at the end of a leaf spring or "cantilever" to the sample. As a raster-scan drags the tip over the sample, a detection apparatus measures the vertical deflection of the cantilever, which indicates the local sample height. In non-contact mode, the AFM derives topographic images from measurements of attractive forces; the tip does not touch the sample [138]. A Q-Scope 250 Quesant AFM with intermittent-contact mode was used for characterization of microcapsules with no polymer, with enzyme encapsulated within, and with polymerization within.

## CHAPTER 5

### RESULTS AND DISCUSSIONS

#### **5.1 Fabrication of (PEM)s and Encapsulation of HRP Within Capsules**

Four bilayers of PSS and PAH [(PSS/PAH)<sub>4</sub>] were assembled on MF-cores as indicated in Chapter 3. Figure 5.1 shows the alternation of  $\zeta$  potential with the adsorption of each polyelectrolyte layer onto the MF cores. The assembly is repeatable, stable, and follows the general scheme of alternate adsorption of oppositely charged polyelectrolytes [139, 140]. After core dissolution (Figure 5.2a), hollow shells have a diameter of about 4.5  $\mu\text{m}$  and exhibit some shrinkage when compared with the parent MF cores (5.0  $\mu\text{m}$  diameter). Encapsulation of (HRP) in the capsules was the first step towards achieving polymerization in the capsules. When pH of the bulk HRP solution, in which the capsules were suspended, was adjusted to 4.0 there was an increase in shell permeability. This effect would have resulted in “openings” in the wall of the capsules that allow permeation of HRP into the capsules. Conversely, when the pH was adjusted to 8.5, there was “closing” of the capsules’ wall leaving HRP trapped in the walls and within the capsules [141]. Figure 5.2b shows the capsules after encapsulation of FITC-labeled HRP. The confocal intensity profiles of both empty and filled capsules taken across their equatorial plane confirm uniform encapsulation of capsules with HRP (Figure 5.2)

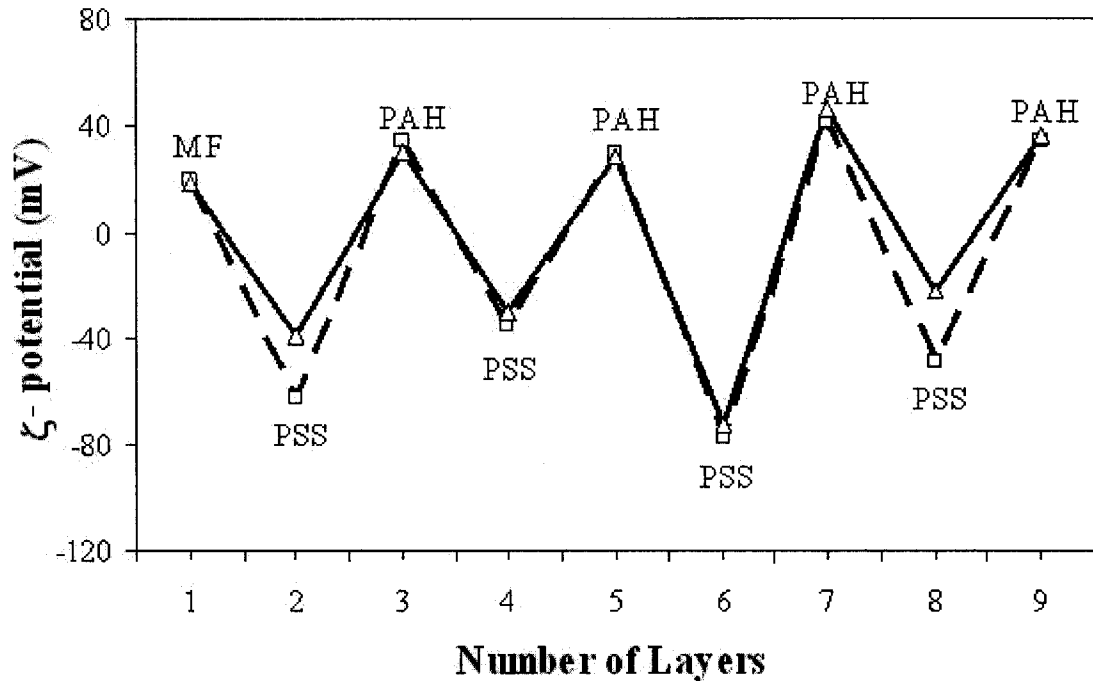


**Figure 5.1:  $\zeta$  potential of polyelectrolytes coated MF particles vs. the number of adsorbed layers. The dashed and solid lines represent data of two independent experiments on assembling (PSS/PAH)<sub>4</sub> layers on MF cores**

### **5.2 Polymerization Catalyzed by HRP Within Microcapsules**

Because of their low molecular weight, tyramine and H<sub>2</sub>O<sub>2</sub> permeated freely into the capsules already loaded with HRP. Polymer formation was effected both within the capsules' interior and in the polyelectrolyte walls where all the three reagents (tyramine, hydrogen peroxide and catalyst-HRP) were present. We assume that the polymer with relatively long polymer chains remains inside the capsules due to the selective permeability of the capsule walls [142]. Capsule walls are not permeable to molecules with molecular weight higher than 4,000, which corresponds in our case to polymerization degree for tyramine of 24. Residual polymer formation in free solution could have been effected by the presence of trace amounts of HRP released from

capsules. The capsules with the polymer inside were washed several times with DI water to remove traces of unreacted monomer,  $H_2O_2$ , peroxidase and oligomers in bulk solution.

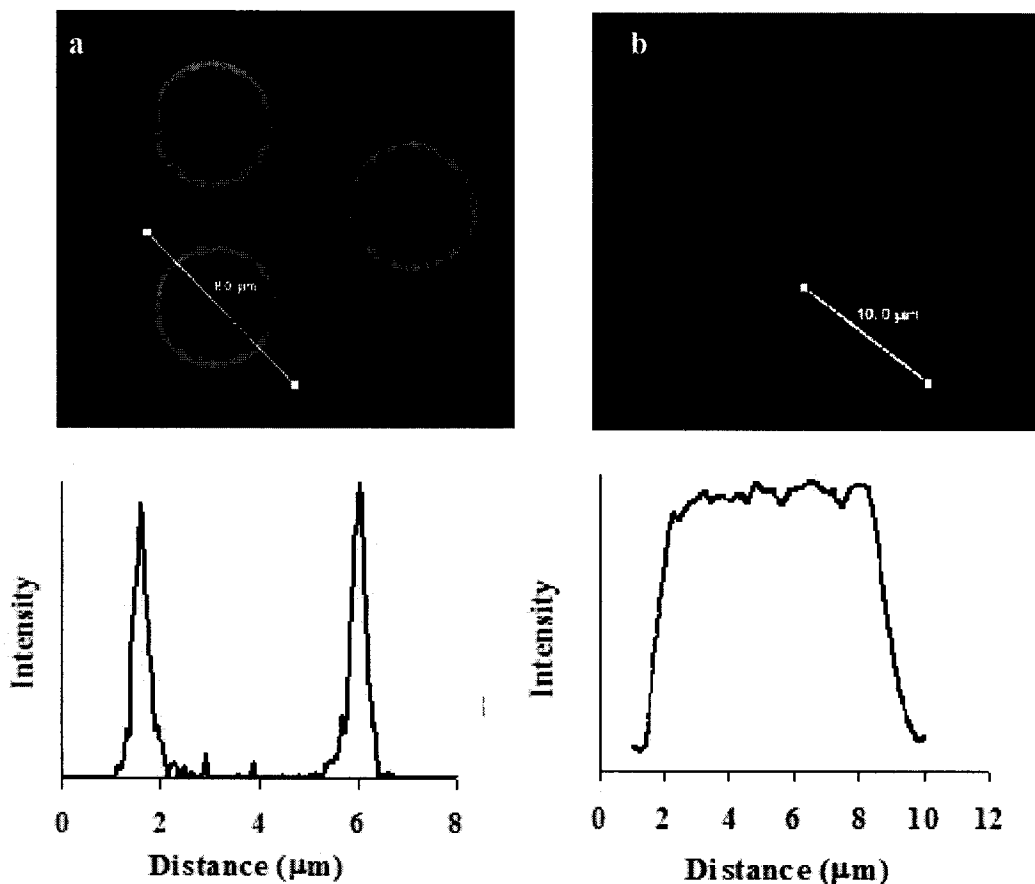


**Figure 5.2: (a) Confocal images of hollow  $(PSS/PAH)_4$  capsules obtained after core dissolution (FITC was added to the suspension to visualize the capsules and (b) capsules loaded with HRP labeled with FITC, as well as corresponding intensity profiles across the equatorial plane of the capsules**

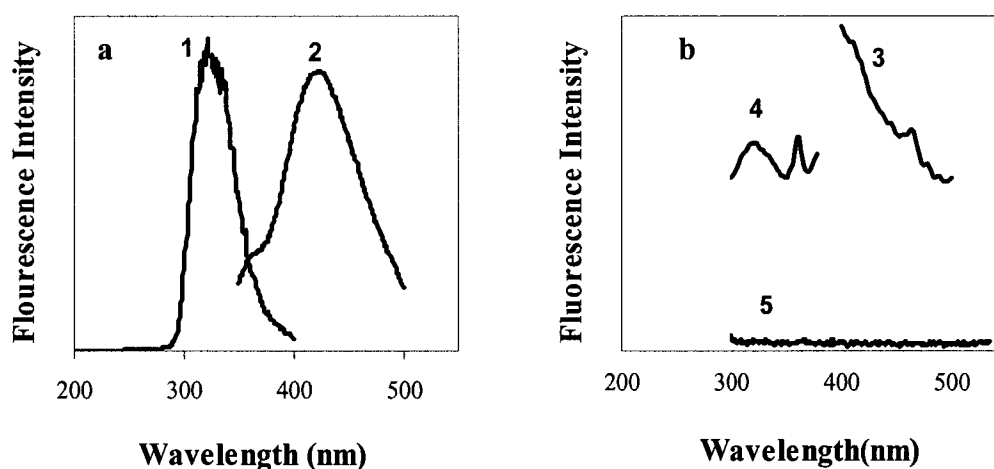
Peroxidase-catalyzed polymerization of phenol and its derivatives usually produce a polymer with a complicated structure. The main structure is composed of repeating phenylene units or a mixture of phenylene and oxyphenylene [143-148]. Due to radical resonance along the phenolic ring, one-electron oxidation of oxyphenol activates ortho

and para positions of the phenolic ring making them additional radical centers for chain propagation [144]. Formation of numerous coupling products and polymers depends on the structure of the monomer used and the presence of additives providing templates for specific attachment of the monomer before polymerization [148]. The polymer formed has a structure composed of several conjugated bonds contributing to its fluorescent nature, and in the case of several phenol polymers, the formation of fluorescent products was demonstrated [143, 149-151]. The absorption and emission band of such polymers has been detailed elsewhere [143]. In some cases, a long tail of fluorescence in the visible range was found because of formation of fluorescent groups. Since the fluorescence is very sensitive and even trace amounts of such groups in a polymer backbone can be recorded, it is possible to monitor synthesis of such polymers.

The fluorescence spectrum of the polymer formed in free solution from its corresponding monomer appears as shown in Figure 5.3a. The excitation and emission wavelengths for the polymer in free solution are 294 and 408 nm respectively, a result which is in good agreement with results (326 and 410 nm) reported in the literature [149,150]. For polymer inside the polyelectrolyte capsules, the emission characteristic (for excitation at 321 nm) was as shown in Figure 4b. There is no prominent maximum intensity peak, but an exponential decline of emission with increasing wavelength was found. However, an inconspicuous peak at 414 nm can be seen which corresponds to the emission peak of polymer in free solution. We believe that presence of phenolic groups in polyelectrolytes like PSS used for construction of hollow capsules may result in considerable noise in the emission spectrum of polymer confined within capsules as well as in unexpected peaks. Tails of absorption and emission in the visible range of spectra



were found, which allowed use of confocal microscopy for visualization of capsules containing fluorescent polymer. It has to be mentioned that synthesis in submicron volume often yields products with a structure different from that found in bulk solution [143]. In this case, phenol polymer was formed in the presence of relatively high amount of proteins and in the vicinity of charged polyelectrolyte surfaces, which can affect the morphology of the polymer and its optical properties. For example, for polyaniline formed in presence of poly(styrene sulfonate) a 200-nm shift of adsorption maximum to the higher wavelength was found [148]. Emission spectrum of empty shells (Figure 5.3b) is practically flat except for very feeble intensity maxima at 360 nm, which is very close to the excitation wavelength of 320 nm and can be attributed to Raman effects.



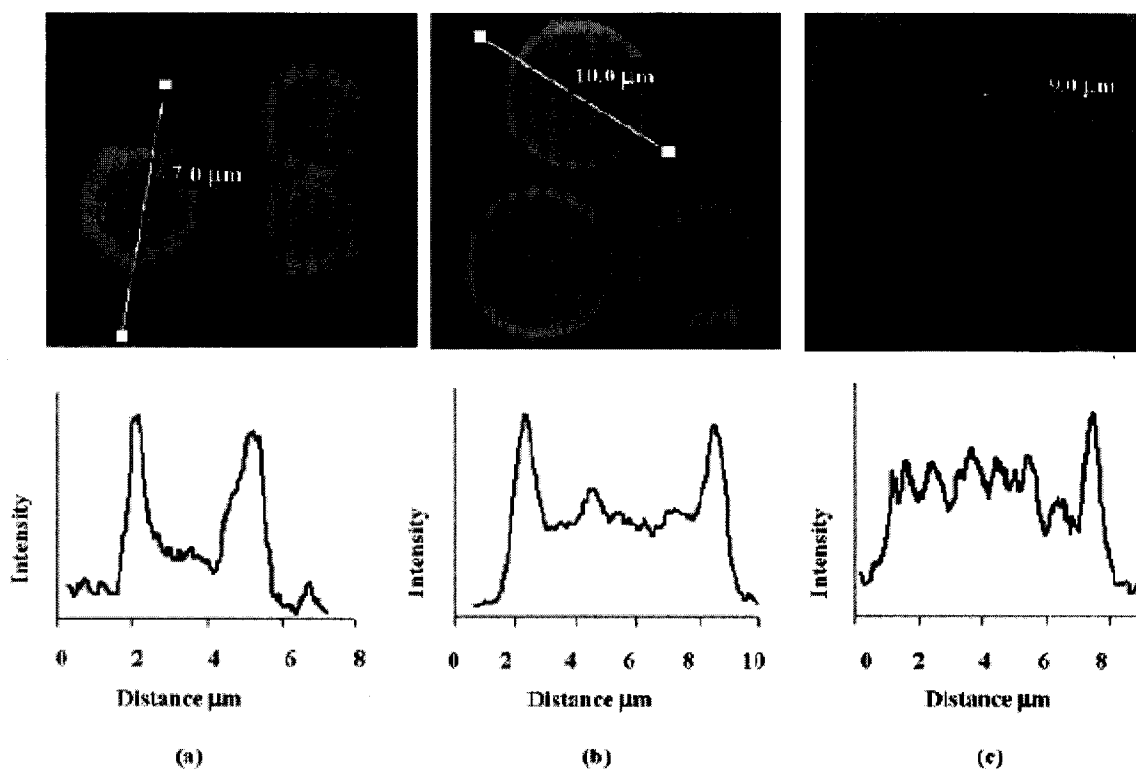
**Figure 5.3: Emission and excitation spectra: (a) polymer formed in bulk solution where curve (1) represents the excitation characteristic and curve (2) represents the emission characteristic; (b) excitation and emission spectra where curve (3) represents emission characteristic for polymer formed within shells (excited at 321nm), (4) represents emission characteristics for HRP-FITC encapsulated within shells (excited at 488 nm), and (5) represents emission for empty shells (excited at 320 nm)**

Figure 5.4a and b show confocal images and intensity profiles for capsules filled with polymer formed at different concentrations of monomer. The effect of monomer concentration was checked by carrying out polymerization at tyramine concentrations of 4 mg/mL and 60 mg/mL. One can see that the relative intensity of fluorescence is more pronounced at the walls of the capsules as compared to the capsules' interior. It may be due to (1) higher adsorption of catalyst (HRP) within capsule walls, (2) adsorption of the polymer formed inside capsule onto the walls, or (3) different structure and optical characteristics of the polymer formed on polyelectrolyte layers. In the case of higher monomer concentrations, higher ratio of fluorescence intensity at the wall to that in the interior was obtained. Therefore, the amount of polymer formed in the walls as well as in the interior of the capsules increases with the increase in monomer concentration. Brighter spots of 400 nm diameter are visible in the capsule cross-sectional image (Figure 5.4c), which indicate polymer nucleation.

For better understanding the morphology of the polymer formed in the capsules, fluorescein isothiocyanate (FITC) was used to stain the capsules filled with polymer (Figure 5.4c). The distribution appears to be in the form of small "islets" within the capsules. The noticeable formation of these "islets" began 40-50 min after addition of  $H_2O_2$  to the reaction mixture. No patterning was found if only tyramine was added to the capsules loaded with peroxidase.

The dimensions of the islets are about 400 nm in diameter, and their appearance can be attributed to increasing hydrophobicity of material within the capsules with formation of rather hydrophobic phenolic polymer, which prevents delivery of the monomers to the reaction zone. It should be mentioned that HRP acts as the catalyst and

a template for the polymerization, and that the polymer is formed at tyrosine sites of HRP [141].



**Figure 5.4: Confocal images of capsules with polymer formed in situ at different concentration of monomer: (a) - 4 mg/ml; (b) - 60 mg/ml and corresponding intensity profiles. (c) - same as (b) but additionally labeled with FITC**

The AFM image of hollow capsules (Figure 5.5) shows that the total height of the folded and dried four-bilayer capsule is about 20 nm. The thickness of a capsule with peroxidase encapsulated inside increased to 40 nm, indicating that extra material is included inside. Considering the shape of dried capsule to be a cylinder and assuming the density of solid residue of polymer and protein as ca.  $1.1 \text{ g/cm}^3$ , the mass of a hollow capsule can be estimated as  $0.5 \times 10^{-12} \text{ g}$ . The mass of HRP loaded in the capsule is ca.  $0.7 \times 10^{-12} \text{ g}$ . CLSM gives the diameter of such capsule in solution of about  $7.0 \text{ μm}$  and its volume is  $1.8 \times 10^{-10} \text{ cm}^3$ . Therefore, the concentration of peroxidase inside the

capsule is about 4.1 mg/mL. It is larger than the initial peroxidase concentration used for the loading (1.5 mg/mL) and indicates accumulation of the protein inside the capsules. Similar protein accumulation was observed for polyelectrolyte capsule loading with hemoglobin and glucose oxidase. Loading with initial 0.5 mg/mL resulted in 25-30 mg/mL protein concentration in the capsule [141]. The mechanism for a protein concentration increase inside the capsules is not obvious. It may be connected with asymmetrical diffusion in and out of the capsules due to asymmetry in the capsule wall having a negative inner surface (PSS) and positive outermost surface (PAH). Consider the AFM image of dried polymer-loaded capsule (Figure 5.5c).

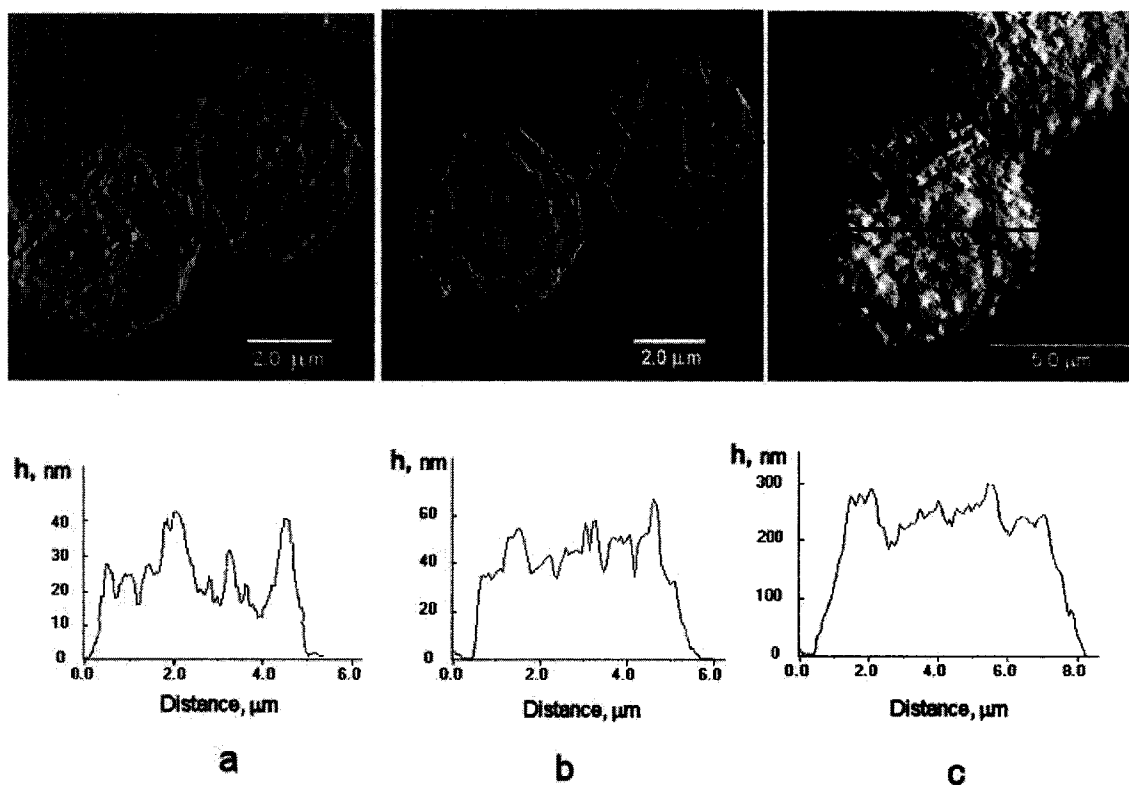


**Figure 5.5: AFM images of capsules and height profiles of one of the capsules: (a) hollow, (b) filled with HRP, and (c) after polymerization of tyramine inside the capsules**

The diameter of the capsule filled with polymer is 7.5 mm, its cross section is  $44.2 \times 10^{-8} \text{ cm}^2$ , and the height in dry state is 240 nm (i.e., much more than thickness of empty capsules, Figure 5.5a). Therefore, the volume of a dried capsule containing polymer is  $10.6 \times 10^{-12} \text{ cm}^3$ , and its mass is  $11.7 \times 10^{-12} \text{ g}$  (if density of solid residue is considered as  $1.1 \text{ g/cm}^3$ ). From these values, one can calculate that the mass of polymer formed in the capsule is  $10.4 \times 10^{-12} \text{ g}$ ; this value is one order of magnitude higher than the amount of peroxidase loaded in one capsule, which is evidence of occurring polymerization. This conclusion is also confirmed by the results obtained by using QCM and confocal microscopy. The evaluated mass of a dry capsule increases from ca.  $\sim 10^{-12} \text{ g}$  for empty and HRP loaded capsules to  $>10^{-11} \text{ g}$  after polymerization. In the case of 30 mg/mL initial tyramine concentration, the amount of monomer in one 7.5mm diameter capsule should reach  $6.6 \times 10^{-12} \text{ g}$ , assuming equilibrium with bulk concentration. In comparison with the polymer mass calculated within a microcapsule ( $10.4 \times 10^{-12} \text{ g}$ ), it appears that additional tyramine participates in the polymerization reaction diffusing into the capsules from the surrounding solution during the polymerization. Different explanations can be proposed for the fact that the amount of the polymer remaining inside the capsules is smaller than the amount of bulk monomer available for polymerization. All capsules occupy less than 1.5% of total volume of the solution, meaning that not all tyramine was polymerized. One of the reasons for the deceleration of the reaction at this stage may be the blocking of peroxidase catalytic centers with formed polymers [148, 149]. Indirect experimental evidence for this phenomenon may be the formation of islets with increased density within capsules composed possibly from HRP-polymer complexes. The sealing of the walls with newly formed polymer which then prevents

penetration of tyramine molecules inside the capsules should also be considered. Permeability of the walls for oligomers with molecular weight lower than several thousand could also result in the loss of some polymeric materials.

### **5.3 Papain Assembly and Polymerization on QCM Resonator**

Four bilayers of (PSS/PDDA) were deposited on a QCM resonator as precursor layers. Alternate assembly of (PSS/PDDA)<sub>4</sub>/ PSS ensured uniform coverage of the QCM resonator substrate with uniform coverage. With its isoelectric point between pH 8.0 and 9.5, Papain can be assumed to be positively charged at pH 6.5 (this was the pH at which Papain was used for assembly) [118, 119]. The deposition of each layer of Papain was indicated by a positive increase in thickness, which confirmed our assumption, and that Papain can be assembled with precision thickness in the range of 3-4 nm per step of growth. Figure 5.6 represents the measured change in thickness plotted against number of layers. The total thickness of the films deposited for of (PSS/PDDA)<sub>4</sub>/ PSS/ Papain/PSS)<sub>10</sub>/Papain is approximately 45 nm. The assembly was also found to be repeatable and stable for the sequence, (PSS/PDDA)<sub>4</sub>/ PSS/ Papain/PSS)<sub>5</sub>/Papain (Figure 5.7).

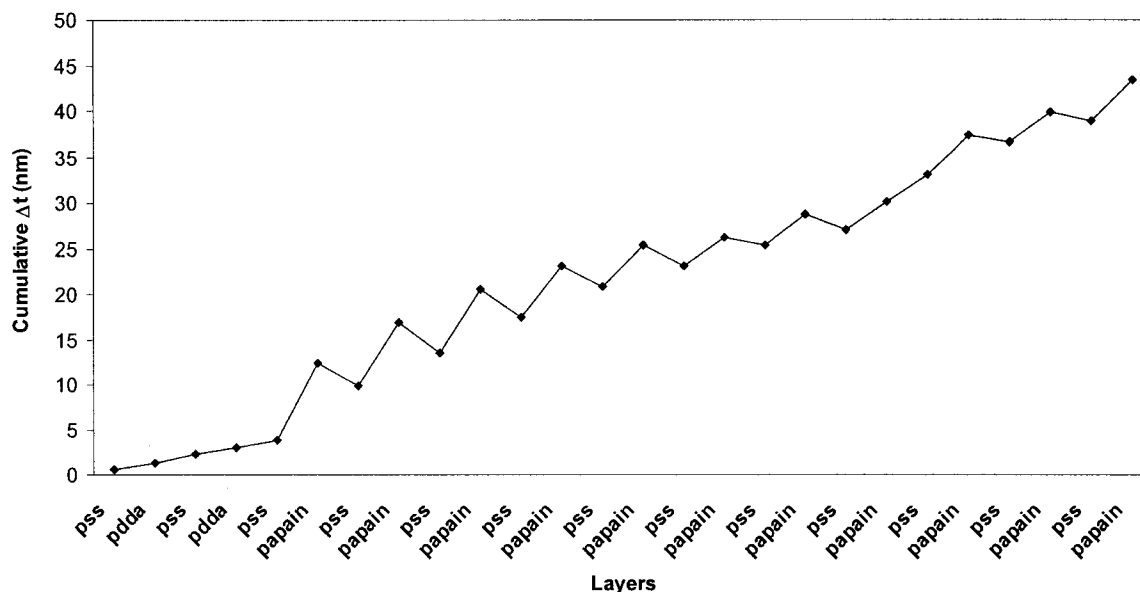


**Figure 5.6: QCM characterization showing thickness variation with deposition of each monolayer of (PSS/PDDA)<sub>4</sub>/(PSS)/(Papain/PSS)<sub>10</sub>(Papain)**

In another experiment, assembly of (PSS/PDDA)<sub>4</sub>/PSS/Papain/PSS)<sub>5</sub>/Papain was achieved. This resonator was then immersed in phenylalanine (monomer) solution (120 mg/mL) and heated in a water bath at 40°C for 7.5 h. The change in thickness was monitored after 1.5h and 7.5 h subsequent to polymerization. As seen from Figure 5.7, a decrease in thickness was observed followed by a sharp increase after 7.5 h indicating that polymerization was effected and that the polymer formed was deposited on the QCM resonator. We believe that the decrease in thickness (c.a ~ 10 nm) was a result of “compaction” of layers due to the extended heating. Polymerization is initiated in 3 h and proceeds linearly with time [118], corresponding to the sharp increase in thickness (Figure 5.7)

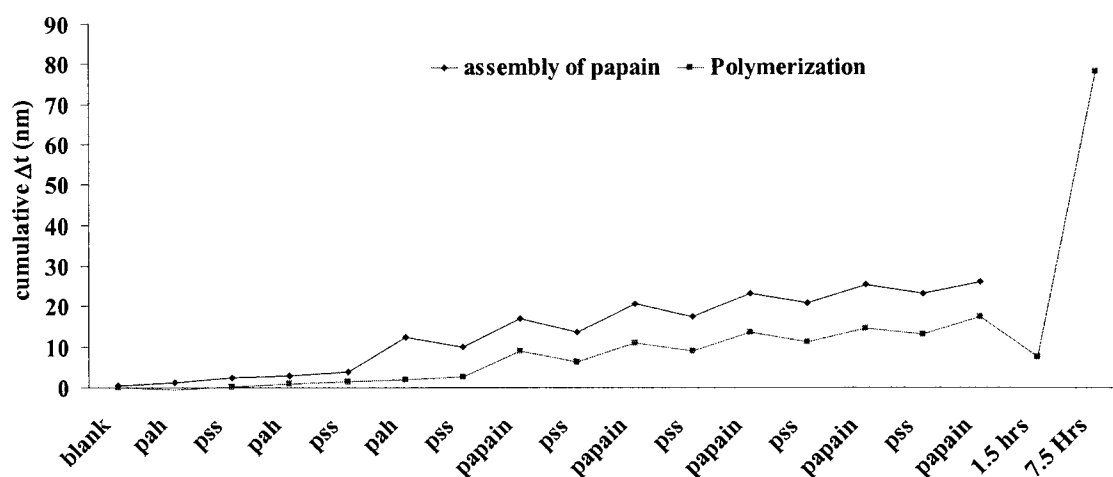


**Figure 5.7: QCM monitoring of change in thickness with assembly of Papain on resonator before and after polymerization. Two separate experiments were conducted with two different resonators: one for assembly of Papain and one for assembly of Papain followed by polymerization**

#### 5.4 Papain Assembly on $\text{MnCO}_3$ Cores

Two bilayers of  $(\text{PSS}/\text{PAH})_2$  followed by three bilayers of  $(\text{PSS}/\text{Papain})_3$  were assembled on  $\text{MnCO}_3$  cores as described in Chapter 3. Figure 5.8 shows the alternation of  $\zeta$  potential with the adsorption of each layer onto the cores.  $\text{MnCO}_3$  cores possess uniform positive charge in the monodispersed state. After assembly of the first layer of PSS, which is negatively charged polyelectrolyte, the charge on the  $\text{MnCO}_3$  cores becomes negative as is indicated by the  $\zeta$ -potential (-30 to -70 mV) (Figure 5.8). Thereafter, with the deposition of each PAH and PSS layer deposition, charge alternation is observed. After  $(\text{PSS}/\text{PAH})_3/(\text{PSS})$ , the  $\text{MnCO}_3$  cores possess an overall negative surface charge. Deposition of the first layer of Papain results in alternation of the  $\zeta$ -potential to +25 to +40 mV indicating that Papain is positively charged and that it can be assembled alternately with PSS. Alternate assembly of  $(\text{Papain}/\text{PSS})_2/(\text{Papain})$  was successfully



achieved with the outermost layer being Papain. The assembly is repeatable and stable for four different sets of experiments conducted independently (Figure 5.8). In a separate set of experiments, FITC- Papain was employed for assembly [(PSS/PAH)<sub>2</sub>/(PSS/Papain)<sub>3</sub>] on MnCO<sub>3</sub> cores in order to confirm the deposition of papain on the cores via CLSM characterization. Figure 5.9 shows a CLSM image of cores with FITC-Papain assembled on them. FITC-Papain was deposited uniformly only on the outer surface of all the cores, as indicated by the fluorescence intensity profile taken across the equatorial plane of one of the capsules (Figure 5.9b). No change in the structural conformation of the cores was observed.

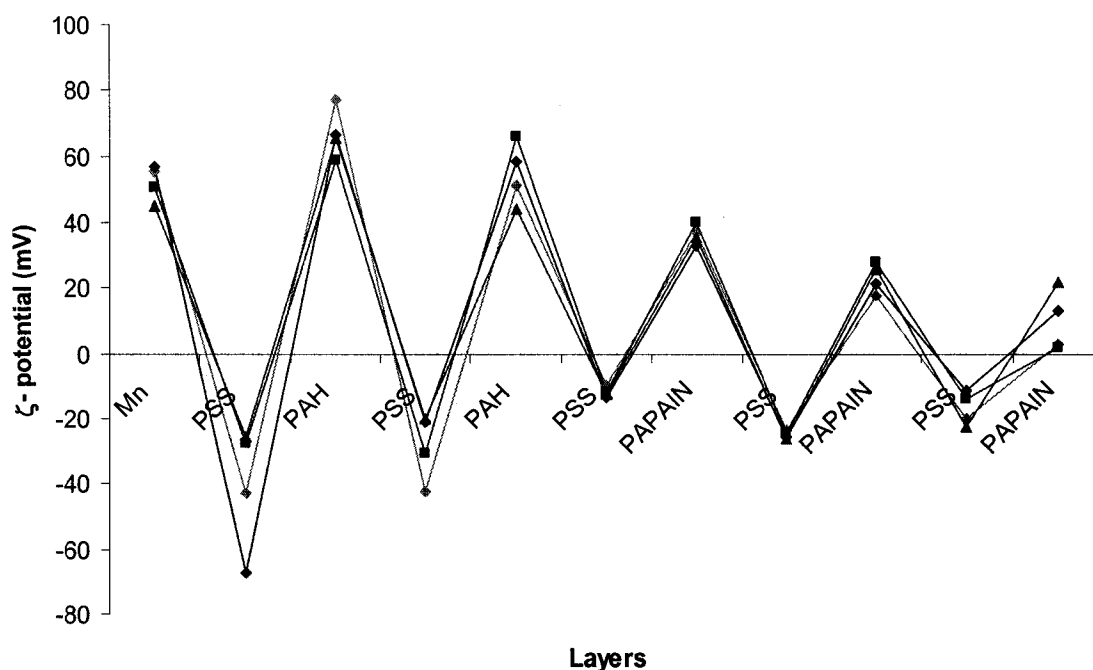


**Figure 5.8:  $\zeta$ - potential monitoring of assembly of (PSS/PAH)<sub>2</sub>/(PSS/Papain)<sub>3</sub> on MnCO<sub>3</sub> particles (d = 6.2  $\mu$ m)**

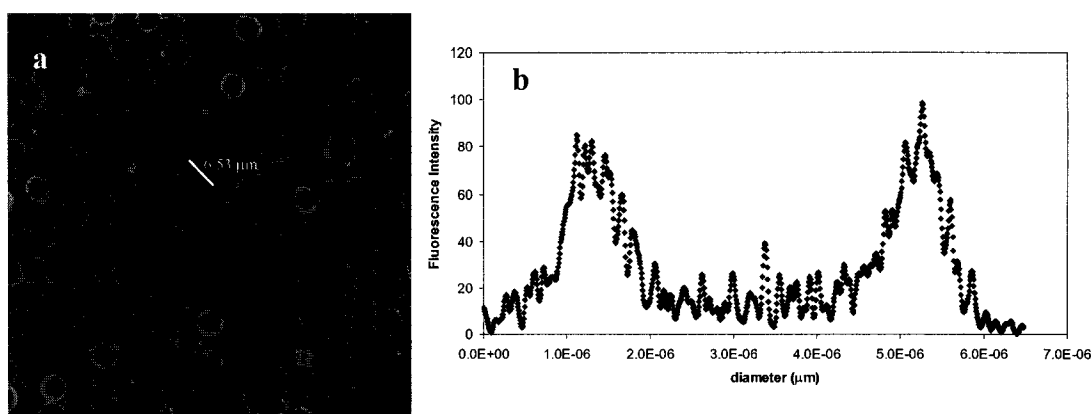


**Figure 5.9: (a) CLSM image of MnCO<sub>3</sub> capsules with (PSS/PAH)<sub>4</sub> / (PSS/FITC-Papain)<sub>3</sub> and (b) CLSM image showing intensity variation across the equatorial plane**

### **5.5 Polymerization of Phenylalanine Catalyzed by Papain Assembled on MnCO<sub>3</sub> Cores**

MnCO<sub>3</sub> cores with [(PSS/PAH)<sub>2</sub> / (PSS/FITC-Papain)<sub>3</sub>] were prepared, and polymerization was effected on the cores, as described in Chapter 3. After 6 hours of heating at 40°C with constant stirring, the sample was washed several times with DI water to remove traces of unreacted phenylalanine and polyphenylalanine that formed in bulk solution. CLSM characterization showed that the enzyme assembled on the surface of the cores had permeated into the cores (Figure 5.10a). This result can be confirmed by the intensity profile taken across the equatorial plane of the cores after polymerization (Figure 5.10b). We believe that this phenomenon is due to formation of polyphenylalanine on the surface of the cores. The distribution of FITC-Papain is uniform on the surface of the MnCO<sub>3</sub> cores (Figure 5.9). As the enzyme catalyzes the formation of peptide bonds between phenylalanine molecules, insoluble particles of

polyphenylalanine are formed which are insoluble in water. These particles form at the active sites of the enzyme and with time, occupy more surface area, thereby forcing the FITC-Papain into the  $\text{MnCO}_3$  cores.  $\text{MnCO}_3$  cores are not known to be porous in nature. However, the combination of two factors namely, (1) heating at  $40^\circ\text{C}$  over an extended period of time and (2) insoluble polypeptide formation at active sites of the enzyme assembled on the cores may result in pore formation within the cores.

In a separate experiment,  $\text{MnCO}_3$  cores with  $[(\text{PSS}/\text{PAH})_2/(\text{PSS}/\text{FITC-Papain})_3]$  which were heated in DI water, in the absence of phenylalanine, at  $40^\circ\text{C}$  for 6 hours showed no noticeable change with respect to the distribution of the FITC-Papain assembled on the cores was concerned. Therefore, we concluded that the unique conformation of the FITC-Papain for the case of cores on which polymerization was effected, was indeed due to the formation of the polypeptides on the surface of the  $\text{MnCO}_3$  cores. (Figure 5.11)

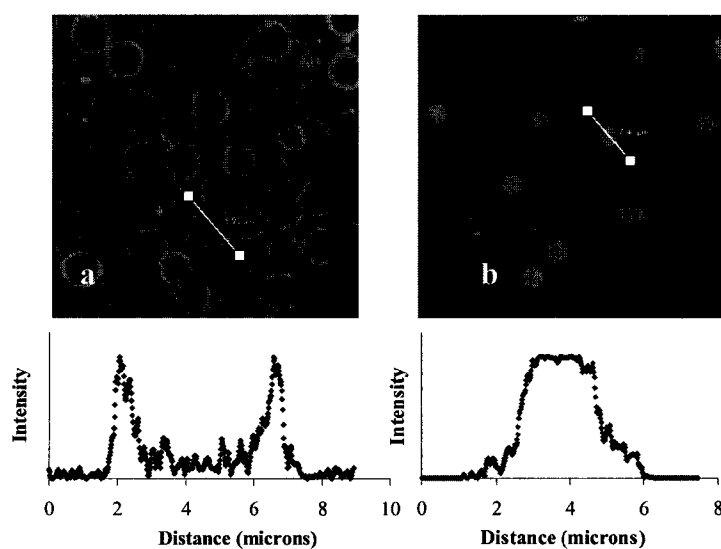


**Figure 5.10: (a)CLSM image of FITC-Papain assembled on  $\text{MnCO}_3$  cores and intensity profile across equatorial plane, (b)CLSM image of  $\text{MnCO}_3$  cores with FITC-Papain assembled on them, after polymerization with intensity profile across the equatorial plane**

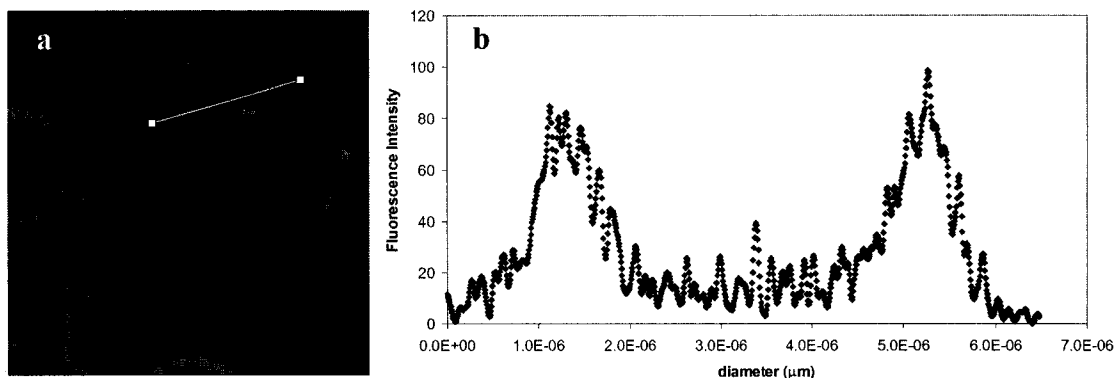


**Figure 5.11: (a) CLSM image of  $\text{MnCO}_3$  cores with FITC-Papain assembled on them after heating in DI water at  $40^\circ\text{C}$  for 6 hours, (b) with intensity profile across the equatorial plane**

### **5.6 Encapsulation of Papain Within $(\text{TA}/\text{CHW})_5$ Microcapsules**

TA/CHW capsules were fabricated using the procedure described in Chapter 3 and used for encapsulating Papain. When the pH of the bulk rhodamine-Papain solution in which the capsules were suspended was adjusted to 5.0, increase in shell permeability occurred. This effect could have resulted in “openings” in the walls of the capsules that allow permeation of HRP into the capsules. Conversely, when the pH was adjusted to 8.5, there was “closing” of the capsules’ wall leaving rhodamine-Papain trapped in the walls and within the capsules [141]. The principle behind encapsulating Papain is the same as that for encapsulating HRP. Figure 5.12 shows the capsules after encapsulation of Rhodamine-labeled Papain. The confocal intensity profiles of both empty  $(\text{TA}/\text{CHW})_5$  and filled capsules taken across their equatorial plane confirm nearly uniform encapsulation of capsules with Papain (Figure 5.13, Figure 5.14)

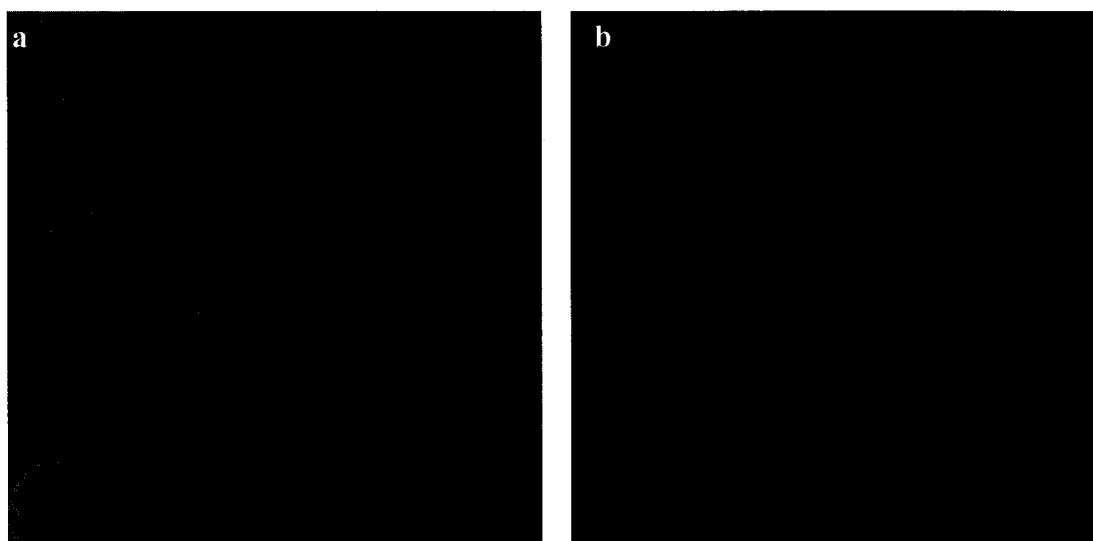


**Figure 5.12: (a) CLSM image of empty (Tannic Acid/ Chitosan)<sub>5</sub> capsules and (b) (Tannic Acid/ Chitosan)<sub>5</sub> capsules loaded with Rhodamine-labeled Papain**

The loading was estimated as  $((F_{\min} - F_0)/(F_{\max} - F_0)) \times 100\%$ , where  $F_{\max}$ ,  $F_{\min}$ , and  $F_0$  were the signal intensities from the walls and interior of the capsule and that from outside the capsule obtained from a fluorescence profile taken along the capsule cross-section. The extent of filling of the capsules is estimated from this formula c.a ~ 60%.

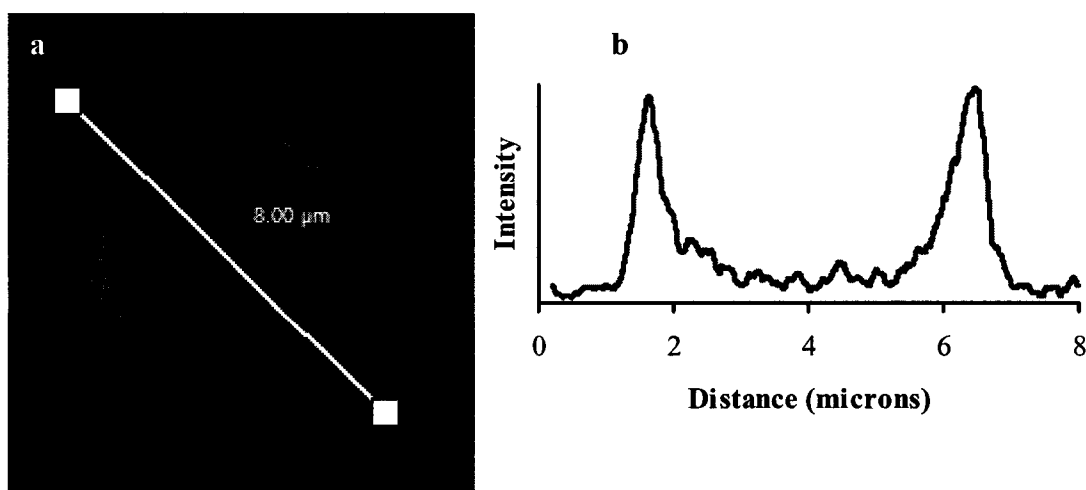


**Figure 5.13: (a) High magnification CLSM image of empty (Tannic Acid/ Chitosan)<sub>5</sub> capsule; (b) CLSM intensity profile across equatorial plane of the capsule**

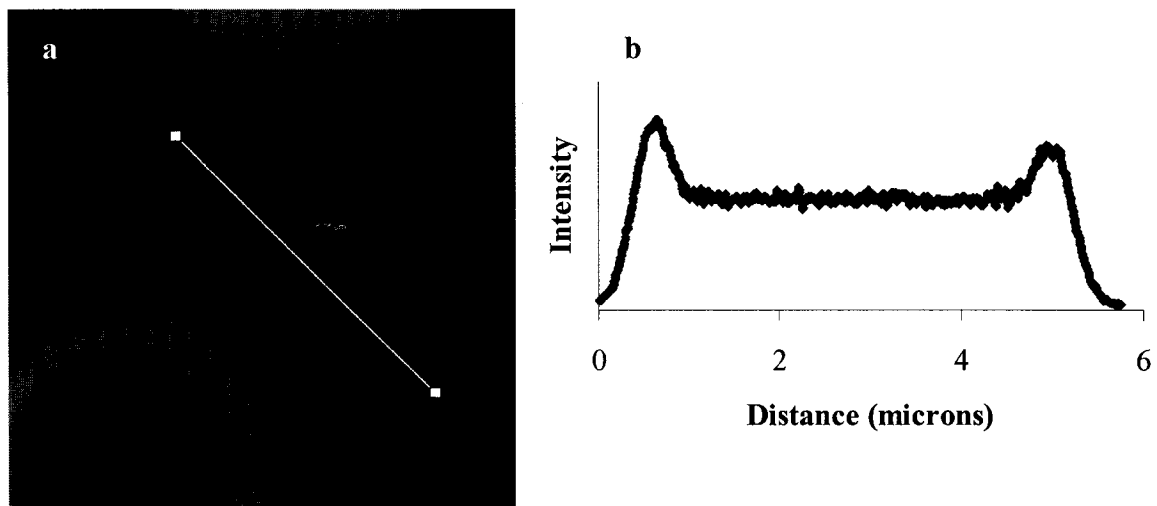


**Figure 5.14: (a) High magnification CLSM image of two (Tannic Acid/ Chitosan)<sub>5</sub> capsules loaded with Rhodamine-labeled Papain; (b) CLSM intensity profile across equatorial plane of a capsule**

## CHAPTER 6

### CONCLUSIONS AND RECOMMENDATIONS

#### 6.1 Conclusions

HRP encapsulated capsules formed via LbL have been successfully utilized for synthesizing polymer within the capsules. We have presented a general method for polymer incorporation in capsules using small monomers, which can easily penetrate the capsule wall. The captured polymers exhibit fluorescent properties, allowing for selective light-guided addressing of the capsules. The polymers are formed both on the wall and inside the capsules with the polymer being more concentrated at the walls than in the interior of the capsules. Monomer concentration has proven to be one of the degrees of freedom for the polymerization reaction. As the monomer concentration was increased, the extent to which the capsules were filled with polymer increased significantly.

Fabrication of polyelectrolyte capsules using  $\text{MnCO}_3$  cores was achieved. Papain assembly on  $\text{MnCO}_3$  cores was achieved and polymerization was effected on the outer surface of the cores. Fabrication of (TA/CHW)<sub>5</sub> microcapsules was achieved and these capsules were successfully used for encapsulating papain within. Due to the capability of encapsulation of biochemical catalysts such as enzymes, there are limitless possibilities for reactions that can be carried out within these microcapsules.

Modified capsules can be used as fluorescent microparticles for immunoassays, nanoreactors for chemical synthesis, and sensory applications. The formation of biocatalyst-rich pools in continuous water phase can be formed within microcapsules. The encapsulation of enzymes within the microcapsules opens up limitless possibilities for construction of new types of nanocomposites with desirable properties in biologically friendly environment.

### **6.2 Recommendations for Future Work**

Polymerization on  $\text{MnCO}_3$  cores with papain assembled on them was achieved. For this work, CLSM characterization was the only method used to study the process. Although there is a perceptible and unique change in the distribution of the FITC-papain assembled on the  $\text{MnCO}_3$  cores which is observable only after polymerization, there is no direct proof of the presence of polymer on the cores. Therefore, we plan to label the end-groups of the peptide using fluorescent peptide-labels in order to visualize the polyphenylalaline forming on the cores. We also plan to use other methods such as UV-Vis, Fluorescence Spectrophotometry, AFM, and Matrix-Assisted Laser Desorption Ionization (MALDI) mass spectroscopy for further characterization of the polypeptides synthesized both on the cores as well as within TA/CHW microcapsules. We intend to follow the same methodology for characterizing polypeptides within microcapsules as was undertaken successfully for polymerization using HRP.

One possible future endeavor could entail experimentation in the direction of characterizing sequenced polypeptide formation using different monomers within microcapsules. This would enable fabrication of microcapsules loaded with sequenced



polypeptides and their sustained release in certain cases when the sequenced polypeptide encapsulated within microcapsules possesses therapeutic properties.

Also several reaction parameters that can be used as degrees of freedom in order to study the behavior of the polymerization system include

- Temperature
- pH of monomer solution
- Concentration of monomer
- Enzyme concentration encapsulated within microcapsules or on the outer surface of microcapsules
- Time of heating

Enzyme kinetics can be studied by applying Michaelis-Menten modeling, which will provide more insight into the dynamics of the polymerization reaction allowing one to control key parameters and optimize the yield of the resulting product. By modifying certain factors, it can also be possible to synthesize products with different properties.

## REFERENCES

1. Decher G, Hong JD, Schmitt J., “ Buildup of ultrathin multilayer films by a self-assembly process”, *Thin Solid Films*, 1992, 210, pp. 831-835
2. Decher G., “Fuzzy nanoassemblies: toward layered polymeric multicomposites”, *Science*, 1997, 277, 1232 -1237
3. Decher G, Eckle M, Schmitt J, Struth B., “ Layer-by-layer assembled multicomposite films”, *Curr. Opin. Coll. Interface Sci.*, 1998, 3, 32 -39
4. Hammond P.T., “ Recent explorations in electrostatic multilayer thin filmassembly”, *Curr. Opin. Coll. Interface Sci.*, 1999, 4, 430-442.
5. Bertrand P, Jonas A, Laschewsky A, Legras R., “ Ultrathin polymer coatings by complexation of polyelectrolytes at interfaces: suitable materials, structure and properties”, *Macromol. Rapid Commun.*, 2000;21:319 –48.
6. Sukhorukov GB, Donath E, Lichtenfeld H, et al., “ Layer-by-layer self assembly of polyelectrolytes on colloidal particles”, *Coll. Surf. (a), Physicochem. Eng. Aspects*, 1998, 137, 253-266
7. Donath E, Sukhorukov GB, Caruso F, Davis SA, Mohwald H., “Novel hollow polymer shells by colloid-templated assembly of polyelectrolytes”, *Angew. Chem. Int. Ed.*, 1998, 37, 2202-2205
8. Schönhoff M, “Self-Assembled Polyelectrolyte Multilayers”, *Current Opinion in Colloid and Interface Science*, 8, 2003, 86–95

9. Decher, G.; Hong, J. D. *Macromol. Chem., Macromol. Symp.*, 1991, 46, 321
10. Decher, G.; Lehr, B.; Lowack, K.; Lvov, Y.; Schmitt, J. *Biosens. Bioelectron.* 1994, 9, 677
11. Lvov Y.; Ariga K.; Kunitake, T. *J. Am. Chem. Soc.* 1995, 117, 6117.
12. Sukhorukov, G. B.; Donath, E.; Davis, S. A.; Lichtenfeld, H.; Caruso, F.; Popov, V. I.; Mo"hwald, H. *Polym. Adv. Technol.* 1998, 9, 759.
13. Donath, E.; Sukhorukov, G. B.; Caruso, F.; Davis, S. A.; Mo"hwald, H. *Angew. Chem., Int. Ed. Engl.* 1998, 37, 2202.
14. Sukhorukov, G. B.; Donath, E.; Lichtenfeld, H.; Knippel, E.; Knippel, M.; Budde, A.; Mo"hwald, H. *Colloids Surf. A* 1998, 137, 253.
15. Gleb B. Sukhorukov,\* ,† Milan Brumen,‡ Edwin Donath,† and Helmuth Mo lhwald, "Hollow Polyelectrolyte Shells: Exclusion of Polymers and Donnan Equilibrium", *J. Phys. Chem. B* 1999, 103, 6434-6440
16. In Protein Architecture: Interfacing Molecular Assemblies and Immobilization Biotechnology; Lvov, Y., Mo"hwald, H., Eds.; Marcel Dekker: New York, 2000.
17. Guesdon, J. L.; Avrameas, S. In *Applied Biochemistry and Bioengineering*; Wingard, L. B., Katchalski-Katzir, E., Goldstein, L., Eds.; Academic Press: New York, 1981; Vol. 3, p 207
18. Turko, I. V.; Yurkevich, I. S.; Chashchin, V. L. *Thin Solid Films* 1992, 210/211, 710.
19. Ahlers, M.; Mu" ller, W.; Reichert, A.; Ringsdorf, H.; Venzmer, J. *Angew. Chem., Int. Ed. Engl.* 1990, 29, 1269
20. Edmiston, P. L.; Saavedra, S. S. *J. Am. Chem. Soc.* 1998, 120, 1665.

21. Decher, G.; Hong, J. D. *Ber. Bunsen-Ges. Phys. Chem.* 1991, 95, 1430.
22. Onda, M.; Ariga, K.; Kunitake, T. *J. Biosci. Bioeng.* 1999, 87, 69
23. Onda, M.; Lvov, Y.; Ariga, K.; Kunitake, T. *Biotechnol. Bioeng.* 1996, 51, 163.
24. Onda, M.; Lvov, Y.; Ariga, K.; Kunitake, T. *J. Ferment. Bioeng.* 1996, 82, 502.
25. Caruso, F.; Niikura, K.; Furlong, D. N.; Okahata, Y. *Langmuir* 1997, 13, 3427.
26. Voigt, A.; Lichtenfeld, H.; Sukhorukov, G.; Zastrow, H.; Donath, E.; Ba"umler, H.; Mo"hwald, H. *Ind. Eng. Chem. Res.* 1999, 38, 4037
27. Caruso, F.; Caruso, R.; Mo"hwald, H. *Science* 1998, 282, 1111
28. Sukhorukov, G.; Donath, E.; Moya, S.; Susha, A.; Voigt, A.; Hartmann, J.; Mo"hwald, H. *J. Microencapsulation* 2000, 17, 177.
29. Antipov, A.; Sukhorukov, G.; Donath, E.; Mo"hwald, H. *J. Phys. Chem.* 2001, 105, 723.
30. Sukhorukov, G.; Antipov, A.; Voigt, A.; Donath, E.; Mo"hwald, H. *Macromol. Rapid Commun.* 2001, 22, 44.
31. Mendelson, J.; Barrett, C.; Chan, V.; Pal, A.; Mayes, A.; Rubner, M. *Langmuir* 2000, 16, 5017.
32. Yuri Lvov,\*;† Alexei A. Antipov,‡ Arif Mamedov,§ Helmuth Mo"hwald,‡ and
33. Gleb B. Sukhorukov\*, "Urease Encapsulation in Nanoorganized Microshells", *Nano Lett.*, Vol. 1, No. 3, 2001, 125-128
34. Jones, J. B. Enzymes in organic synthesis. *Tetrahedron* 42, 3351–3403 (1986).
35. Sih, C. J. & Wu, S. H. Resolution of enantiomers via biocatalysis. *Topics Stereochem.* 19, 63–125(1989).

36. Wong, C.-H. & Whitesides, G. M. *Enzymes in Synthetic Organic Chemistry* (Pergamon, Oxford, 1994).
37. Drauz, K. & Waldmann, H. *Enzyme Catalysis in Organic Synthesis* (Wiley, Weinheim, 1995).
38. Koeller K& Wong C, "Enzymes for Chemical Synthesis", *Nature*, 409, 2001, 232-240
39. Sukhorukov G, Susha A, Davis S, Leporatti S, Donath E, Hartmann J, Mohwald H, "Precipitation of inorganic salts into hollow micron-sized polyelectrolyte shells", *J. Colloid Interf. Sci.*, 2002, 247, 251-254
40. Sukhorukov, G. B.; Da'hne, L.; Hartmann, J.; Donath, E.; Mo'hwald, H. *Adv. Mater.* 2000, 12, 112.
41. Moya, S.; Sukhorukov, G. B.; Auch, M.; Donath, E.; Mo'hwald, H. *J. Colloid Interface Sci.* 1999, 216, 297.
42. Dahne L, Leporatti S, Donath E, Mohwald H, "Fabrication of Microcages with Tailored Propoerties", *J. Am. Chem. Soc.* 2001, 123, 5431-5436
43. E. Fischer, *Ber. Dtsch. Chem. Ces.* 27, 3189 (1894)
44. J. B. S. Haldane, *Enzymes* (Longmans, Green, London, 1930)
45. L Pauling, *Nature* 161, 707 (1948)
46. R. Wolfenden, C. Ridgway, G. Young, *J. Am. Chem. Soc.* 120, 833 (1998)
47. W. R. Cannon, S. J. Benkovic, *J. Biol. Chem.* 273, 26257 (1998).
48. W. R. Cannon, S. F. Singleton, S. J. Benkovic, *Nature Struct. Biol.* 3, 821 (1996)
49. A. Warshel, *Proc. Natl. Acad. Sci. U.S.A.* 81, 444 (1984)
50. F. H. Westheimer, *Adv. Phys. Org. Chem.* 21, 1 (1985).

51. W. P. Jencks, *Chem. Rev.* 72, 705 (1972).
52. T. C. Bruice, *Annu. Rev. Biochem.* 45, 331 (1976)
53. A. Warshel, *Proc. Natl. Acad. Sci. U.S.A.* 75, 5250 (1978).
54. Uyama, H.; Kobayashi, S. *Chemtec* 1999, *October*, 22-28
55. Uyama, H.; Kurioka, H.; Kaneko, I.; Kobayashi, S. *Chemistry Letters* 1994, 423-426
56. Uyama, H.; Kurioka, H.; Kobayashi, S. *Chemistry Letters* 1995, 795-796
57. Uyama, H.; Kurioka, H.; Sugihara, J.; Komatsu, I.; Kobayashi, S. *Bull. Chem. Soc. Jpn.* 1995, 68, 3209-3214
58. Uyama, H.; Kurioka, H.; Sugihara, J.; Kobayashi, S. *Bull. Chem. Soc. Jpn.* 1996, 69, 189-193
59. Uyama, H.; Kurioka, H.; Sigihara, J.; Kobayashi, S. *Colloids and Surfaces A: Physiochemical and engineering Aspects* 1999, 153, 189-194
60. Uyama, H.; Takeya, K.; Hoshi, N.; Kobayashi, S. *Macromolecules* 1995, 28, 7046-7050
61. Noda, S.; Kamiya, N.; Goto, M.; Nakashio, F. *Biotech. Letters* 1997, 19, 307-309
62. Ichinohe, D.; Muranaka, T.; Sasaki, T.; Kobayashi, M.; Kise, H. *J. Polym. Sci.: Part A: Polym. Chem.* 1998, 36, 2593-2600
63. Kobayashi, S.; Shoda, S.; Uyama, H. *Adv. Polym. Sci.*, 1995, 121, 1.
64. Kobayashi, S.; Shoda, S.; Uyama, H. In *Catalysis in Precision Polymerization*; Kobayashi, S., Ed.; John Wiley & Sons: Chichester, 1997, Chapter 8.
65. Ritter, H. In *Desk Reference of Functional Polymers, Syntheses and Applications*; Arshady, R., Ed.; American Chemical Society: Washington, 1997, pp. 103-113.
66. Gross, R.A.; Kaplan, D.L.; Swift, G. (Ed.) *ACS. Symp. Ser.*, 1998, 684.

67. Kobayashi S.; Uyama, H. In *Materials Science and Technology, Synthesis of Polymers*; Schlüter, A.-D., Ed.; Wiley-VCH: Weinheim, 1998, Chapter 16.
68. Joo, H.; Yoo, Y. J.; Dordick, J. S. *Korean J. Chem. Eng.* 1998, *15*, 362.
69. Kobayashi, S. *J. Polym. Sci., Polym. Chem. Ed.*, 1999, *37*, 3041.
70. Kobayashi, S.; Uyama, H.; Ohmae, M. *Bull. Chem. Soc. Jpn.* 2001, *74*, 613.
71. Gross, R. A.; Kumar, A.; Kalra, B. *Chem. Rev.* 2001, *101*, 2097.
72. Kobayashi, S.; Uyama, H.; Kimura, S. *Chem. Rev.* 2001, *101*, 3793.
73. Kopf, P. W. In *Encyclopedia of Polymer Science and Engineering*, 2nd Ed., John Wiley & Sons: New York, 1986, vol. *11*, pp45-95
74. Ayyagari, M.; Akkara, J. A.; Kaplan, D. L. *Acta Polymerica* 1996, *47*, 193.
75. Uyama, H.; Kobayashi, S. *CHEMTECH* 1999, *29(10)*, 22.
76. Akkara, J. A.; Ayyagari, M. S. R.; Bruno, F. F. *Trends Biotechnol.* 1999, *17*, 67.
77. Kobayashi, S.; Uyama, H.; Tonami, H.; Oguchi, T. Higashimura, H.; Ikeda, R.; Kubota, M. *Macromol. Symp.* 2001, *175*, 1.
78. Dordick, J. S.; Marletta, M. A.; Klibanov, A. M. *Biotechnol. Bioeng.* 1987, *30*, 31.
79. Hay, A. S. *J. Polym. Sci., Polym. Chem. Ed.* 1998, *36*, 505.
80. Uyama, H.; Kurioka, H.; Kaneko, I.; Kobayashi, S. *Chem. Lett.* 1994, 423.
81. Uyama, H.; Kurioka, H.; Sugihara, J.; Kobayashi, S. *Bull. Chem. Soc. Jpn.* 1996, *69*, 189.
82. Liu, W.; Cholli, A. L.; Kumar, J.; Tripathy, S.; Samuelson, L. *Macromolecules* 2001, *34*, 3522-3526.
83. Samuelson, L.; Anagnostopoulos, A.; Alva, K.; Kumar, J.; Triphany, S. *Macromolecules* 1998, *31*, 4376-4378.

84. Wang, P.; Dordick, J. S. *Macromolecules* 1998, *31*, 941-943.
85. Wang, P.; Martim, B.; Parita, S.; Rethwisch, R.; Dordick, J. *J. Am. Chem. Soc.* 1995, *117*, 12885-12886.
86. Alva, K.; Kumar, J.; Marx, K.; Tripathy, S. *Macromolecules* 1997, *30*, 4024-4029.
87. Banerjee, S.; Premchandran, R.; Tata, M.; John, V.; McPherson, G. *Ind. Eng. Chem. Res.* 1996, *35*, 3100-3107.
88. Banerjee, S.; Ramannair, P.; Wu, K.; John, V.; McPherson, G.; Akkara, J.; Caplan, D. *Enzymes in Polymer Synthesis*; American Chemical Society: Washington, DC, 1998; pp 125-143.
89. Sukhorukov, G. *Dendrimers. MML Series*; Citus Books: New York, 2002; Vol. 5, pp 111-147.
90. Lvov, Y.; Lu, Z.; Schenkman, J.; Rusling, J. *J. Am. Chem. Soc.* 1998, *120*, 4073-4080.
91. Lvov, Y.; Antipov, A.; Mamedov, A.; Mo"hwald, H.; Sukhorukov, G. *Nano Lett.* 2001, *1*, 125-128.
92. Tiourina, O.; Antipov, A.; Sukhorukov, G.; Lvov, Y.; Mo"hwald, H. *Macromol. Biosci.* 2001, *1*, 209-214.
93. Caruso, F.; Trau, D.; Mo"hwald, H.; Renneberg, R. *Langmuir*, 2000, *16*, 1485
94. Gao, C.; Liu, X.; Shen, J.; Mo"hwald, H. *Chem. Commun.* 2002, 1928-1930.
95. Antipov, A.; Shchukin, D.; Fedutik, Y.; Zhanaveskina, I.; Klechkovskaya, V.; Sukhorukov, G.; Mo"hwald, H. *Macromol. Rapid Commun.* 2003, *24* (3), 274-277.
96. Tatsiana Shutava,† Zhiguo Zheng,† Vijay John,‡ and Yuri Lvov, *Biomacromolecules*, 2004, (check for page numbers)



97. Spell, E.; Hopman, A.; Komminoth, P. *J. Histochem. Cytochem.* 1999, 47 (3), 281-288.
98. Townshend, A.; Li, Y.-Z. *Anal. Chim. Acta* 1998, 359 (1-2), 149-156.
99. Guilbault, G.; Brignac, P.; Juneau, M. *Anal. Chem.* 1968, 40 (8), 1256-1262.
100. Guilbault, G.; Brignac, P.; Zimmer, M. *Anal. Chem.* 1968, 40 (1), 190-197.
101. Buchanan, I.; Nicell, J. *J. Chem. Technol. Biotechnol.* 1998, 72, 23- 32.
102. Buchanan, I.; Nicell, J. *J. Chem. Technol. Biotechnol.* 1999, 74, 669-674.
103. H.-D. Jakubke, *Angew. Chem. Int. Ed. Engl.* 34 (1995) 175-177.
104. B. Zhang, T.R.Cech, *Chemistry & Biology* 5 (1998) 539-553.
105. M. Bergmann, H. Fraenkel-Conrat, *J. Biol. Chem.* 119 (1937) 707-720.
106. H.-D. Jakubke, P. Kuhl, A. Kvnnecke, *Angew. Chem. Int. Ed. Engl.* 24 (1985) 85-93.
107. W. Kullmann, *Enzymatic Peptide Synthesis*, CRC Press: Boca Raton ( 1987).
108. H.-D. Jakubke, In: *The Peptides: Analysis, Synthesis, Biology*, S. Udenfried, J. Meienhofer, Eds., Academic Press: New York,(1987),Vol.9, Chapter 3.
109. H.-D. Jakubke, In: *Enzyme Catalysis in Organic Synthesis*, Drauz, K., Waldmann,H., Eds., VCH: Weinheim, (1995),Vol. I, p. 431-458.
110. H.-D. Jakubke, U. Eichhorn, M. Hdnsler, D. Ullmann, *Biol. Chem.* 377 (1996) 455-464.
111. Mohanty A, Misra M, Hinrichsen G, *Macromol. Mater. Eng.*, 2000, 276/277, 1
112. Sanda F, Endo T, *Macromol. Chem. Phys.*, 1999, 200, 2651
113. Imanshi Y., In "Ring-Opening Polymerization", Ivin K, Saegusa T, Elsevier: London, 1984, Chapter 8

114. Kumar A, Gross R, *Biomacromolecules*, 2000, 1, 133
115. Malak, C.A.A., Filippova, I., Yu, Lysogorskaya, E.N., Anisimova, V.V., Lavrenova, G.I. & Stepanov, V.M. (1992) Pepsin as a catalyst of peptide synthesis. Enzyme co-precipitation with emerging peptide products. *Int. J. Peptide Protein Res.* 39, 443±449.
116. Abdel Malak, C.A.A., Lavrenova, G.I., Lysogorskaya, E.N., Filippova, I., Yu, Terent'eva, E. & Yu. & Stepanov, V.M. (1993) Synthesis of tetrapeptide, p-nitroanilides catalyzed by pepsin. *Int. J. Peptide Protein Res.* 41, 97±101.
117. Abdel Malak, C.A.A. (1992) Calf chymosin as a catalyst of peptide synthesis. *Biochem. J.* 288, 941±943.
118. Antonov, V.K. (1977) *Acid Proteases. Structure, Function and Biology* (Tang, J., Ed.), Plenum Press, London, pp. 170±198.
119. Powers, J.C., Harley, A.D. & Myersin, D.V. (1977) *Acid Proteases. Structure, Function and Biology* (Tang, J., ed.). Plenum Press, London pp. 141±157.
120. Malak A, "Pepsin as a catalyst for peptide synthesis: formation of peptide bonds not typical for pepsin substrate specificity", *J. Peptide Res.*, 53, 1999, 606-61
121. D. Silvano, S. Krol, A. Diaspro, O. Cavalleri, A. Gliozzi, *Microsc. Res. Tech.* 2002, 59, 536.
122. Ghan, R.; Shutava, T.; Patel, A.; John, V. T.; Lvov, Y, "Enzyme-Catalyzed Polymerization of Phenols within Polyelectrolyte Microcapsules", *Macromolecules*, 2004, 37(12); 4519-4524
123. Onda, M.; Lvov, Y.; Agira, K.; Kunitake, T. *Biotechnol. Bioeng.* 1996, 51, 163.
124. Gao, C.; Liu, X.; Shen, J.; Mo"hwald, H. *Chem. Commun.* 2002, 1928.

125. Shchukin, D. G.; Radtchenko, I. L.; Sukhorukov, G. B. *Mater. Lett.* 2003, 57, 1743.
126. Shchukin, D. G.; Radtchenko, I. L.; Sukhorukov, G. B. *J.Phys. Chem. B* 2003, 107, 86.
127. Sukhorukov, G. B.; Susha, A. S.; Davis, S.; Leporatti, S.; Donath, E.; Hartmann, J.; Mothwald, H. *J. Colloid InterfaceSci.* 2002, 247, 251.
128. Sophiannikova, M.; Radchenko, I.; Sukhorukov, G.; Shchukin, D.; Yakimansky, A.; Ilnytskyi, Y. *J. Chem. Phys.* 2003, 118, 9007.
129. Lvov, Y.; Ariga, K.; Ichinose, I.; Kunitake, T. *J. Am. Chem. Soc.* 1995, 117, 6117-6122.
130. Rozzell J, Wagner F, " Biocatalytic Production of Amino Acids and Derivatives", Hanser Publishers, Muenchen, 1992
131. G. Snooke, "Investigation of Solid--State Reactions by Electrochemical and Quartz Crystal Microbalance Measurements" PhD thesis, Monash University, Australia, 2000, pp.55--84
132. Sauerbrey, G, "Verwendung von Schwingquarzen zur Wägung dünner Schichten und zur Mikrowägung", *Zeitschrift für Physik*, 155, 1959, pp. 208
133. "Instruction manual for 90 Plus particle sizer", Brookhaven Instruments Corporation, Holtsville, New York, USA, 1995
134. Cheng, P. C., Lin, T.H., Wu, W. L., and Wu, J. L., eds. (1994). "Multidimensional Microscopy." Springer Verlag, New York
135. Haughland, R. P. (1992). "Molecular Probes: Handbook of Fluorescent Probes and Research Biochemicals

136. Guilbault, G. G. Practical Fluorescence. Modern Monographs in Analytical Chemistry. 3: 1990.
137. Binnig, G., Quate, C.F., and Gerber, Ch. (1986) Atomic force microscope. Phys. Rev. Lett. 56(9), 930-933
138. Albrecht, T.R., Akamine, S., Carver, T.E., and Quate, C.F. (1990) Microfabrication of cantilever styli for the atomic force microscope. J. Vac. Sci. Technol. A 8(4), 3386-33
139. G. Decher, *Science*, 1997, v.227, 1232-1237 "Fuzzy nanoassemblies: Toward layered polymeric multicomposites"
140. M. Onda, Y. Lvov, K. Agira, T. Kunitake Sequential Reactions by glucose oxidase/ peroxidase molecular films assembled by layer-by-layer alternate adsorption // *Biotechnol Bioeng* 1996 v.51 163-166.
141. Sukhorukov, G.B., Antipov, A.A., Voigt, A., Donath, E., and Möhwald, H. "pH-controlled macromolecule encapsulation in and release from polyelectrolyte multilayer nanocapsules" *Macromol. Rapid Commun.* 2001, 22, 44-46.
142. G. Sukhorokov, M. Brumen, E. Donath, H. Mohwald, "Hollow Polyelectrolyte Shells: Exclusion of Polymers and Donnan Equilibrium" *J. Phys. Chem., B*, 1999, 6434-6440
143. R.S.Premachandran, S.Banerjee, X.-K.Wu, V.T.John, G.L.McPherson, J Akkara, M.Ayyagari, D.Kaplan Enzymatic Synthesis of Fluorescent Naphtol-Based Polymers. *Macromolecules*, 1996, 29, 6452-6460

144. Liu W., Cholli A.L., Kumar J., Tripathy S., Samuelson L. Mechanistic Study of the Peroxidase-Catalyzed Polymerization of Sulfonated Phenol. *Macromolecules*, 2001, 34, 3522-3526
145. Samuelson L.A., Anagnostopoulos A., Alva K.S., Kumar J., Tripathy S.K. Biologically Derived Conducting and Water Soluble Polyaniline Macromolecules 1998, 31, 4376-4378
146. Wang P., Dordick J.S. Enzymatic Synthesis of Unique Thymidine-Containing Polyphenols// *Macromolecules* 1998, 31, 941-943
147. Wang P., Martim B.D., Parita S., Rethwisch, Dordick J.S. Multienzymatic Synthesis of Poly(hydroquinone) for Use as a Redox Polymer// *J Amer. Chem. Soc.* 1995, 117, 12885-12886
148. Alva K.S., Kuma J., Marx K.A., Tripathy S.K. Enzymatic Synthesis and Characterization of a Novel Water-Soluble Polyaniline: Poly(2,5-diaminobenzenesulfonate)// *Macromolecules* 1997 30, 4024-4029
149. Townshend A., Li Y.-Z. Evaluation of the adsorptive immobilization of horseradish peroxidase on PTFE tubing in flow system for hydrogen peroxide determination using fluorescence detection// *Analytica Chimica Acta* 1998, 359(1-2), 149-156.
150. Guilbault G.G., Brignac P.J., Juneau M. New Substrates for the Fluorometric Determination of Oxidative Enzymes// *Analytical Chemistry* 1968, 40 (8), 1256-1262
151. Guilbault G.G., Brignac P., Zimmer M. Homovanillic Acid as a Fluorometric Substrate for Oxidative Enzymes// *Analytical Chemistry*, 1968, 40(1), 190-197

## **APPENDIX A**

### **SUBSTRATES FOR HORSERADISH PEROXIDASE (HRP)**

## APPENDIX A

Nr.	Substrate	Method	Observations
1	ABTS (2,2'-azino-di[3-ethyl-benzothiazolin-(6)-sulfonate])	spectrophotometric	the method of choice, also used in ELISA
2	pyrogallol	spectrophotometric	(the result is also known as P.Z.-Purpurogallinzahl)
		fluorimetric	
		polarographic	
		titrimetric	
		gasometric	
3	guaiacol	spectrophotometric	
		chronometric	
		titrimetric	
4	hydroquinone	polarographic	the residual H <sub>2</sub> O <sub>2</sub> or substrate concentration are determined
		fluorimetric	the residual hydroquinone is detected with silver halides
		chronometric	together with ascorbate
5	o-tolidine	spectrophotometric	also in ELISA

6	5-aminosalicylic acid	spectrophotometric	also in ELISA
7	o-phenylenediamine	spectrophotometric	also in ELISA; reducing agents such as sulfite stabilize the system by reacting with excess H <sub>2</sub> O <sub>2</sub> after the enzymatic reaction has been terminated
		spectrophotometric	in reversed micelles
		pH changes are measured	
8	p-hydroxybenzenesulfonate	spectrophotometric	coupled to 4-aminoantipyrine
9	4-aminoantipyrine	spectrophotometric	coupled to p-hydroxybenzenesulfonate
		spectrophotometric	coupled to N-ethyl-N-(2-hydroxy-3-sulfopropyl)-m-toluidine
		spectrophotometric	coupled to phenol; also in EIA (Trinder reagent) and also applied for model systems
		spectrophotometric	coupled to N,N-diethylaniline
		spectrophotometric	coupled to 2,4-dichlorophenol



10	3,3',5,5'- tetramethyl- benzidine	spectrophotometric	also in ELISA; surfactants, g -cyclodextrin, penicillin (or derivatives thereof) may be used as additives
			after electrophoresis
11	phenol	EPR	
		spectrophotometric	coupled to 4- aminoantipyrine, in EIA (Trinder reagent)
		spectrophotometric	
12	5-phenyl-4- pentenyl- hydroperoxide (PPHP)	spectrophotometric	selective peroxidase reagent, used together with a reducing substrate
13	fluorescein	fluorimetric	
14	p-anisidine	spectrophotometric	
15	3-methyl-2- benzothiazolin on hydrazone (MBTH)	spectrophotometric	yields an indamine when reacting with m- dimethylaminobenzoic acid
		spectrophotometric	ELISA

16	m-dimethyl-aminobenzoic acid	spectrophotometric	yields an indamine when reacting with MBTH
17	luminol	fluorimetric	in EIA; an impressive number of substances may be used as activators
18	L012 (luminol analog)	fluorimetric	same as above
19	N-ethyl-N-(2-hydroxy-3-sulfopropyl)-m-toluidine	spectrophotometric	coupled to 4-aminoantipyrine
20	3,3'-diaminobenzidine	spectrophotometric	
21	p-phenylene-diamine	spectrophotometric	
22	m-phenylene-diamine	spectrophotometric	
23	pyrocatechin	spectrophotometric	
		polarographic	
		iodometric	enzymatically produced quinone is titrated with iodine

24	o-dianisidine	spectrophotometric	free or dextrane-bound
25	caffeic acid	fluorimetric	
26	ferulic acid	fluorimetric	
27	p-coumaric acid	fluorimetric	
28	coniferyl alcohol	fluorimetric	
29	5-(5'-azoluciferinyl)-2,3-dihydro-1,4-phtalazindione (ALPDO)	fluorimetric	
30	p-hydroxy-phenylpropionic acid	fluorimetric	also in ELISA; alone or together with a surfactant (CTAB or CTAC)
31	homovanillic acid	fluorimetric	o-dianisidine may be used as activator
32	N,N-diethylaniline	spectrophotometric	also coupled to 4-aminoantipyrine; also used for model systems

33	3-amino-9-ethylcarbazole	spectrophotometric	ELISA
34	mesidine	spectrophotometric	
35	ferrocyanide		
36	malachite green	spectrophotometric	
37	guaiac resin	chrometric	
		spectrophotometric	guaiacetic acid is the main product
38	benzidine	chrometric	ascorbate is also needed
		spectrophotometric	
39	2,6-dichlorophenol indophenol	spectrophotometric	
40	2,3',6-trichlorophenol indophenol	spectrophotometric	
41	pyrogalllic acid	spectrophotometric	yields gallopurpurin
42	phenolphthalein	spectrophotometric	

43	o-toluidine	spectrophotometric	
		chronometric	ascorbate is also needed
44	guaiaconic acid	spectrophotometric	
45	p-toluidine	spectrophotometric	
46	acetylguaiacol	spectrophotometric	
47	o-cresol	spectrophotometric	
48	p-cresol	Spectrophotometric	
49	m-cresol	spectrophotometric	
50	a-naphtol	spectrophotometric	also coupled with dimethyl-phenylendiamine (NADI reagent) or with p-phenylendiamine (Guthrie reagent) to yield indophenols
51	aniline	spectrophotometric	
52	ascorbate	spectrophotometric	
		chronometric	iodide, o-toluidine, or benzidine are used as second substrates

53	iodide	chromometric	ascorbate is used as a second substrate
		chromometric	starch, thiosulfate and iodide are also needed
		spectrophotometric or titrimetric	
54	2,7-diaminofluorene	spectrophotometric	
55	p-aminobenzoic acid	spectrophotometric	
56	brilliant green	spectrophotometric	
57	N,N-dimethyl-p-phenylenediamine	spectrophotometric	
58	thymol	spectrophotometric	
59	resorcin	spectrophotometric	
60	orcin	spectrophotometric	
61	fluoroglucine	spectrophotometric	

62	benzoic acid	spectrophotometric	
63	salicylic acid	spectrophotometric	
64	pyrocatechuic acid	spectrophotometric	
65	galic acid	spectrophotometric	
66	adrenaline	spectrophotometric	
67	tyrosine	spectrophotometric	
68	tryptophane	spectrophotometric	
69	flavones	spectrophotometric	
70	2-methyl-6-(p-methoxyphenyl)-3,7-dihydroimidazo[1,2-a]pirazin-3-one	hemiluminescence	luciferin analog
71	acetaminophen and its derivatives	fluorescence	fluorescent 5,5'-diacetamido-2,2'-bisphenol formation

## **APPENDIX B**

### **CHARACTERISTICS OF PAPAIN**



## Appendix B

### Characteristics of Papain from *Carica Papaya*

**Molecular weight:** 23,000

**Composition:** Papain is a single peptide chain of 211 residues folded into two parts that form a cleft. A three-dimensional structure has been indicated. The molecule has one free SH group, which is functional. There are seven subsites each capable of accommodating a single amino acid residue of a peptide substrate.

**Optimum pH:** 6.0 - 7.0.

**Extinction coefficient:**  $E_{278}^{1\%} = 25.0$

**Isoelectric point:** pH 9.6

**Activators:** Papain is activated by cysteine, sulfide, sulfite, etc. It is enhanced when heavy metal binding agents such as EDTA are also present. N-bromosuccinimide enhances the activity of papain.

**Inhibitors:** Substances, which react with sulfhydryl groups including heavy metals, carbonyl reagents. Papain may be inactivated by  $H_2O_2$  generated by [[gamma]]-irradiation of  $H_2O$ - the active SH group being oxidized to sulfenic acid.

**Stability:** Papain as a crystalline suspension is stable at 5°C for 6-12 months. Stabilizing agents are EDTA, cysteine and dimercaptopropanol. To enhance stability as well as solubility it may be advantageous to convert crystalline papain to its mercury derivative.

## **APPENDIX C**

### **LIST OF JOURNAL AND CONFERENCE PUBLICATIONS AND CONFERENCE PRESENTATIONS**

## APPENDIX C

### JOURNAL AND CONFERENCE PUBLICATIONS

1. Tatsiana G.Shutava, **Rohit Ghan**, Zhiguo Zheng, Zonghuan Lu and Yuri M. Lvov, “*Nanoorganized polyelectrolyte microcapsules for Horseradish Peroxidase catalyzed polymer synthesis*”, accepted for publication in *Polym. Mater. Sci. and Eng.*, 2004
2. **R.Ghan**, T.Shutava, A.Patel, V.John, Y.Lvov, “*Enzyme catalyzed polymerization within polyelectrolyte microcapsules*”, *Macromolecules*, 37 (12), pp. 4519 – 4524, 2004
3. T.Shutava, **R.Ghan**, Z.Lu, Y.Lvov, “*Nanoengineered Shells for Encapsulation and Controlled Release*”, *NSF publications*, January 2004
4. R. Khillan, **R. Ghan**, Y. Lvov, Y.Su, “*Layer-by-Layer architecture of nano-films of conductive polymers PEDOT-PSS/ PPy for development of nanoelectronic devices such as LEDs and Transistors*”, accepted for publication in *IEEE Proceedings*, Summer 2004
5. **R.Ghan**, T.Shutava, A.Patel, V.John, Y.Lvov, “*Layer-by-Layer Engineered Microreactors for Bio-Polymerization of 4-(2-aminoethyl) phenol hydrochloride*”, *Mat. Res. Soc. Symp. Proc.*782, pp. A5.43.1 – A5.43.6, 2003
6. **R.C. Ghan**, Y. Lvov, R.S. Besser, “*Characterization of Self-Assembled Tin-Oxide Films for High Sensitivity Micro-Gas Sensors*,” *Mat. Res. Soc. Symp. Proc.*, 707, pp.7.1-7.6, 2002

7. **R.Ghan**, Y. Lvov, R.Besser, "*Uniform Layers for Gas sensor applications*", *Nanoparticle News*, 4(12), Jan 2002, Business Communications Company Inc.

### CONFERENCE PRESENTATIONS

1. **R. Ghan**, T. Shutava, D. Komireddy, Y. Lvov, "*Polyelectrolyte microcapsules as "reactors" for synthesizing bio-polymers*", *American Chemical Society : South West Regional Meeting, (ACS SWRM), Fall 2004, Abstract accepted (poster presentation)*
2. T. Shutava, **R. Ghan**, Z. Lu, Y. Lvov, "Polyelectrolyte Shells for Micro-Confined Biosyntheses of Polymers," *NSF-Conference on Micromanufacturing, Dallas, January 8, 2004*
3. **R.Ghan**, T.Shutava, A.Patel, V.John, Y.Lvov, "*Layer-by-Layer Engineered Microreactors for Bio-Polymerization of 4-(2-aminoethyl) phenol hydrochloride*", *Mat. Res. Soc. Symp. Fall 2003, Poster presentation*
4. **R.C. Ghan**, Y. Lvov, R.S. Besser, "*Characterization of Self-Assembled Tin-Oxide Films for High Sensitivity Micro-Gas Sensors*," *Mat. Res. Soc. Symp, .Fall 2002, Poster presentation*
5. **R.C. Ghan**, Y. Lvov, R.S. Besser, "*Development of a Novel Bio-Gas Sensor for Sensing Carbon Monoxide*," *Abstracts of the BoR EPSCoR Conference, Baton Rouge, Louisiana, 2002*

6. M. Prevot, **R. Ghan**, Y. Lvov, and R.S. Besser, "*The Integration of Silicon Micromachining and Layer-by-Layer Nanoassembly*," Abstracts of the *Tex-MEMS III Conference*, University of Texas and Zyvex Corporation, June 2001
7. M. Prevot, **R. Ghan**, Y. Lvov, R. Besser, "*Integration of Silicon Microfabrication and Layer-by-Layer Nanoassembly*", 2<sup>nd</sup> *Louisiana Microfabrication Conference*, Baton Rouge, Aug 22, 2001